The Meteoritical Society

Meteoritics & Planetary Science 1–22 (2025)
doi: 10.1111/maps.70073

The Qingzhen reaction, a fine-grained mineral assemblage associated with djerfisherite in some EH3 chondrites: Alteration on the EH parent body

Peter Mc ARDLE[1]*, Rhian H. JONES[1], Luke DALY[2,3,4], Romain TARTÈSE[1], Patricia L. CLAY[5], Brian O'DRISCOLL[5], Ray BURGESS[1], William SMITH[6], Colin HOW[6], and Lewis HUGHES[1]

[1]Department of Earth and Environmental Sciences, University of Manchester, Manchester, UK
[2]School of Geographical and Earth Sciences, University of Glasgow, Glasgow, UK
[3]Department of Materials, University of Oxford, Oxford, UK
[4]Australian Centre for Microscopy & Microanalysis, University of Sydney, Camperdown, New South Wales, Australia
[5]Department of Earth and Environmental Sciences, University of Ottawa, Ottawa, Ontario, Canada
[6]School of Physics and Astronomy, University of Glasgow, Glasgow, UK

***Correspondence**
Peter Mc Ardle, Department of Earth and Environmental Sciences, University of Manchester, Manchester M13 9PL, UK.
Email: peter.mcardle@manchester.ac.uk

(Received 13 June 2025; revision accepted 03 November 2025)

Abstract–Enstatite chondrites formed under extremely reducing conditions in the protoplanetary disk. They are derived from two or more parent bodies, EH and EL, and both EH and EL groups contain petrologic type 3–6 samples. The rare lithophile- and halogen-bearing sulfide, djerfisherite, occurs in low abundance in enstatite chondrites, most frequently in the EH3 chondrites. In some EH3 chondrites, but not in EL chondrites, djerfisherite is associated with a fine-grained mineral assemblage, termed the "Qingzhen Reaction," which has previously been interpreted as an alteration product of djerfisherite. The Qingzhen Reaction is notable as perhaps the only record of fluid-mediated alteration on the EH parent body. In this study, we undertook a high-resolution chemical and mineralogical analysis of the Qingzhen Reaction and its djerfisherite host, in order to determine its composition, relationship to djerfisherite and its formation environment. We show that the Qingzhen Reaction is an alteration product of djerfisherite, predominantly comprised of porous troilite with remnant djerfisherite. Trace quantities of halite and (likely) sphalerite are also present. We suggest that the Qingzhen Reaction formed by the interaction of an anhydrous fluid with djerfisherite on the EH parent body.

INTRODUCTION

Enstatite chondrites (ECs) are a rare class of meteorites which formed in the inner region of the early solar system (Kleine et al., 2020). ECs formed under very reducing conditions in the protoplanetary disk, as evidenced by their mineralogy, such as Mg-rich endmember silicates (e.g., enstatite) and lithophile-bearing sulfides (e.g., oldhamite, djerfisherite, niningerite, and alabandite) (Lin, 2022; Weisberg & Kimura, 2012). Despite their inner solar system origin, ECs are enriched in moderately volatile elements compared to CI chondrite abundances (Palme et al., 2014; Rubin & Choi, 2009). The ECs originate from at least two separate parent bodies, EH and EL (Weisberg & Kimura, 2012). The oldest measured chronological dates for ECs are Mn-Cr dates of 4.56 Ga, which record chondrule formation (Zhu et al., 2020). Results from modeling studies suggest the EC parent bodies accreted at c. 1.8 ± 0.1 Ma after the formation of Ca- and Al-rich Inclusions (CAI) (Sugiura & Fujiya, 2014). After accretion, both EH and EL parent bodies were subjected to varying degrees of metamorphism due to radiogenic heating generated by the decay of short-lived isotopes such as ^{26}Al and ^{60}Fe

(Huss et al., 2006). This resulted in a range of petrologic types from 3 (least metamorphosed) to 6 (most metamorphosed) for both EH and EL chondrites. For type 4–6 ECs, Rb-Sr and Ar-Ar systematics record younger dates (e.g., 4.406–4.465; Minster et al., 1979), interpreted as either parent body cooling from internal radiogenic heating or impact resetting. Other heating mechanisms for the ECs, relying on collisional processes, have also been proposed, including impact-induced shock melting (Rubin & Wasson, 2011) and contact metamorphism from impact melt sheets (Gray et al., 2025). There are no known ECs with petrologic types 1–2 (aqueously altered), reflecting a general lack of aqueous alteration on the EH and EL parent bodies. However, the ECs do contain indigenous hydrogen (Barrett et al., 2025; Piani et al., 2020), and rare observations suggest the presence of limited aqueous fluids. Rindlisbacher et al. (2021) and Weisberg et al. (2023) recently found potential evidence of hydrothermal alteration in the anomalous EL3 Northwest Africa (NWA) 8785, evidenced by a magnetite-rich matrix and the presence of sodalite. Additionally, Goss et al. (2023) found evidence of Na metasomatism in the anomalous EL3-related Lewis Cliff (LEW) 87223 meteorite in the form of abundant Al-rich chondrules with both Ca- and Na-plagioclase.

In this study, we focus on the lithophile- and halogen-bearing sulfide djerfisherite [$(K,Na)_6(Fe,Cu,Ni)_{25}S_{26}Cl$] (Clay et al., 2014), and its breakdown in the "Qingzhen Reaction" (QR), which was first described in the Qingzhen EH3 chondrite (El Goresy et al., 1983; El Goresy et al., 1988). Djerfisherite is very common, although not abundant (<1 modal%), in the EH3 (Clay et al., 2014; Ebel & Sack, 2013) and it is also found in some aubrites (Clay et al., 2014; Wilbur et al., 2024). Outside of these meteorites, occurrences of meteoritical djerfisherite are extremely rare, and include the EH5 chondrite St. Mark's (Fuchs, 1966; Ramdohr, 1963), two EL3 chondrites MacAlpine Hills (MAC) 88136 (Lin & El Goresy, 2002) and NWA 8785 (Weisberg et al., 2023), as well as reported rare occurrences in iron meteorites (El Goresy, 1971; Kracher et al., 1977). Notably, no djerfisherite has been found in any EH4, EH6, or EL4-6 meteorites. The apparent absence of djerfisherite in types 4 and 6 ECs, and its absence in all type 5 except St. Mark's, supports the view that it is generally unstable under thermal metamorphic conditions, and that its presence in St. Mark's is anomalous (Brearley & Jones, 2018). We note that a small (c. 1 μm) isolated djerfisherite grain has also been reported from a Ryugu sample (Miyahara et al., 2025).

In the EH3, djerfisherite is usually found as components of polyphase MSN or as solitary grains within the matrix. Various pre-accretionary formation mechanisms have been proposed for djerfisherite in the ECs, including direct condensation from the nebula (Ebel & Sack, 2013) and sulfidization of metal in the nebula (El Goresy et al., 1988; Lin & El Goresy, 2002). However, some djerfisherite (along with other sulfides) in EH3 is also found in veins. Opaque veins in the ECs are usually taken as the product of shock processes (Rubin, 2015). Others have argued that opaque veins (occasionally djerfisherite-bearing) within the EH3 Qingzhen are pre-accretionary, as opposed to being induced by shock (El Goresy et al., 1988; Lin & El Goresy, 2002). Aubritic djerfisherite is clearly a secondary phase: Wilbur et al. (2024) proposed that aubritic djerfisherite formed by alteration of troilite and metal via anhydrous, alkali- and Cl-rich fluid metasomatism.

Although various meteorite types contain djerfisherite, as outlined above, the QR has only been found in EH3 chondrites. In some, but not all, EH3, djerfisherite is associated with a fine-grained mineral assemblage (Figure 1), that is considered to represent a breakdown (the QR) of djerfisherite to predominantly porous troilite, in addition to trace-minor amounts of covellite, idaite, bornite, sphalerite, and other unidentified phases, including an unknown K-bearing phase (El Goresy et al., 1988; Lin & El Goresy, 2002). There are a number of ideas to explain the cause of the QR. El Goresy et al. (1988) suggested that the porous nature of troilite and sphalerite in the QR was a result of volatile loss, leading to the interpretation that the QR resulted from the breakdown of djerfisherite during post-accretion thermal metamorphism. In further work, Lin and El Goresy (2002) observed that troilite in QR occurrences is concentrated along grain boundaries and cracks. They also observed that all djerfisherite occurrences within Qingzhen and Yamato (Y)-691 exhibit the QR, with the notable exception of small djerfisherite inclusions within metal which are QR-free. Based on these observations, Lin and El Goresy (2002) concluded that the QR resulted from interactions of djerfisherite with volatile components, except for metal-hosted djerfisherite that was protected from alteration. However, arguments for the QR taking place during parent body thermal metamorphism (i.e., during heating resulting from decay of short-lived radionuclides within a few million years after accretion) are potentially problematic (Lin & El Goresy, 2002), because of relatively young Ar-Ar and Rb-Sr apparent dates of c. 2 Ga for the QR-bearing meteorites (Hopp et al., 2014; Torigoye & Shima, 1993). Although Qingzhen and Y-691 do not exhibit evidence of significant shock (El Goresy et al., 1988; El Goresy & Ehlers, 1989; Lin & El Goresy, 2002; Rubin, 2015), some authors have interpreted the young apparent dates of the QR-bearing EH3 as evidence of shock-induced chronometer resetting. Despite these

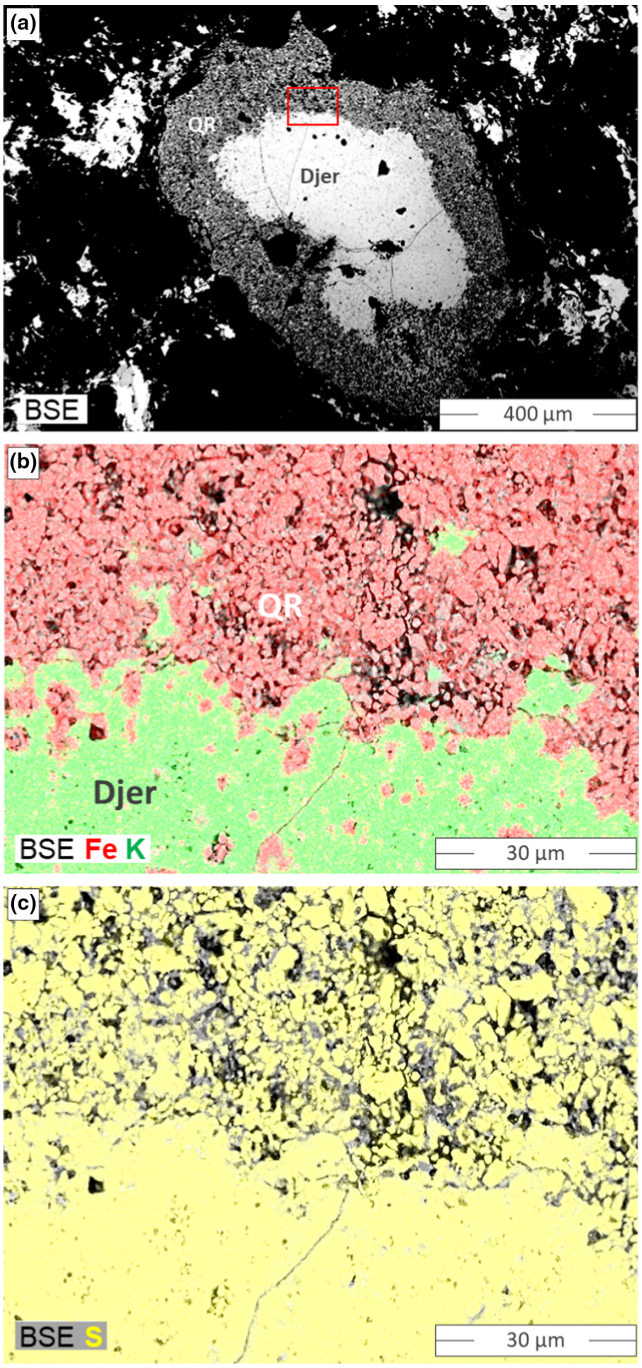

FIGURE 1. (a) Backscattered electron (BSE) image of a solitary djerfisherite (Djer) occurrence in the EH3 Sahara (SAH) 97072, showing an unaltered Djer core surrounded by a fine-grained, porous "Qingzhen-reaction" (QR) zone. (b, c) Higher magnification map of the area outlined in red in (a), showing a composite of BSE and energy dispersive spectroscopy (EDS) elemental maps (Fe: red, K: green in B, and S: yellow in c). In (b), djerfisherite appears green and QR-troilite is red. In (c) note that S is present in djerfisherite and throughout the QR.

works, there is still considerable uncertainty about what process generated the QR.

Interpreting the environment of formation of the QR, along with its cause, depends on a clear understanding of the reaction products and formation mechanism. In order to better understand the nature and reaction mechanism of the QR, and the environment in which it formed, we have investigated the fine-grained mineralogy, chemistry, and texture of the QR using high-resolution techniques including scanning transmission electron microscopy, transmission Kikuchi diffraction, and elemental mapping using laser ablation inductively coupled plasma–mass spectrometry.

METHODS

Samples

Two EH3, Sahara (SAH) 97072 and Northwest Africa (NWA) 13299, are the primary focus of this study (Table 1). Both are QR-bearing EH3 (EH3-QRB), and both are finds from hot desert environments in Africa. Interior to their weathering rinds, the samples of both meteorites examined in this study are minimally weathered, equivalent to weathering grade W0.

Several additional djerfisherite-bearing EH3, EL3 and aubrites were also examined, details of which are given in Table 1. These include Yamato(Y)-691 and Qingzhen, both EH3-QRB, and several non-QR bearing EH3 (EH3-nonQRB): Dominion Range (DOM) 14021, Larkman Nunatak (LAR) 12252, Miller Range (MIL) 07028, Allan Hills (ALHA)77295, and Elephant Moraine (EET) 83322. Additionally, we examined MacAlpine Hills (MAC) 88136, a djerfisherite-bearing EL3 (no QR present) (see Table 1). For all EC samples (except Northwest Africa (NWA) 8785), we assigned our own weathering grades based on the classification scheme of Zurfluh et al. (2016). Our assigned weathering grades may differ compared to previously published weathering grades for the same meteorites. This is because weathering grades can vary in individual meteorites, and our specific samples of the meteorites in this study are unlikely to be the same as those in previous studies. An additional reason for differences in weathering grade classification could be that we have used the scheme of Zurfluh et al. (2016) which may be different from other studies (many studies do not list the weathering classification scheme used). For several EC samples, we determined their shock grade based on the classification of Rubin (2015) (Table 1). Table 1 also summarizes relevant information from the literature for the EL3 NWA 8785 (no QR present), and several aubrites (no QR present), which were not examined as part of this study.

TABLE 1. Summary of djerfisherite-bearing enstatite chondrites and aubrites.

Sample full name	Abbr. name	Samp. no.	Class.[1]	QRB/ nonQRB	Fall/ Find	Shock (Refs.)	Weath. Grade	Samp Source/ Study Refs.
Northwest Africa 13299	NWA 13299	—	EH3	QRB	Find	S3[a]	W0	WWM
Sahara 97072	SAH 97072	—	EH3	QRB	Find	S2[b]	W0	TMM
Yamato 691	Y-691	,124	EH3	QRB	Find	S4[b]	W1	NIPR
Qingzhen		454	EH3	QRB	Fall	S3[b]	W1	UCLA
Larkman Nunatak 12252	LAR 12252	,27	EH3	nonQRB	Find	—	—	ANSMET
Larkman Nunatak 12252	LAR 12252	,29				S2[c]	—	
Larkman Nunatak 12252	LAR 12252	,32				—	W2	
Elephant Moraine 83322	EET 83322	,15	EH3	nonQRB	Find	S3[b]	W2	ANSMET
Dominion Range 14021	DOM 14021	,30	EH3	nonQRB	Find	—	—	ANSMET
Dominion Range 14021	DOM 14021	,33				S2[c]	—	
Dominion Range 14021	DOM 14021	,39				—	W2	
Allan Hills A77295	ALHA77295	,55	EH3	nonQRB	Find	S3[c]	W1	ANSMET
Miller Range 07028	MIL 07028	,7	EH3	nonQRB	Find	—	W3	ANSMET
Miller Range 07028	MIL 07028	,35				—	W2	
Miller Range 07028	MIL 07028	,38				S3[c]	—	
MacAlpine Hills 88136	MAC 88136	,12	EL3	nonQRB	Find	S3[b]	W1	ANSMET
Northwest Africa 8785	NWA 8785	—	EL3	nonQRB	Find	S2[d]	—	1
Allan Hills 84007	ALH 84007	—	Aubrite	nonQRB	Find	—	Ae	2
Peña Blanca Spring		—	Aubrite	nonQRB	Fall	—	—	2, 3
Aubres		—	Aubrite	nonQRB	Fall	—	—	2
Allan Hills 78113	ALH 78113	—	Aubrite	nonQRB	Find	—	A/Be	2,4
Yamato 793592	Y-793592	—	Aubrite	nonQRB	Find	—	—	4

Note: Shock references: [a]Meteoritical Bulletin as of November 30, 2024, [b]Rubin (2015), [c]this study, [d]Rindlisbacher et al. (2021). Weathering grades for chondrites are from this study, based on the classification scheme of Zurfluh et al. (2016), weathering grades for aubrites are from Meteoritical Bulletin as of November 30, 2024, based on the ANSMET weathering scheme. Source of samples: ANSMET—The Antarctic Search for Meteorites/NASA/JSC, NIPR—National Institute for Polar Research, UCLA—University of California Los Angeles Meteorite Collection, WWM—Purchased from F. Kuntz WW Meteorites, TMM—Purchased from E. Twelker, The Meteorite Market. Study references: [1]Rindlisbacher et al. (2021), [2]Wilbur et al. (2024), [3]Clay et al. (2014), [4]Kimura et al. (1993).
Abbreviations: nonQRB - non-Qingzhen Reaction bearing; QRB - Qingzhen Reaction bearing; Samp. no. - sample number; Weath. - weathering.
[1]Classification, Meteoritical Bulletin as of November 30, 2024.

Electron Microscopy Analyses

Prior to, between, and after analyses, samples were stored in a desiccator. Meteorite chips/slices were cut on a wire saw using a deionized water lubricant. Directly afterward, slices were washed in isopropyl alcohol (IPA). Slices were then mounted in epoxy and polished with progressively finer Si-C polishing discs followed by diamond pastes with decreasing granulometry. Polished mounts were then washed in IPA. Scanning electron microscopy with energy dispersive X-Ray spectroscopy (SEM-EDS) analyses were undertaken at the University of Manchester on an FEI/Thermo Fisher Quanta 650 field emission electron microscope, equipped with a Bruker X Flash 6–30 energy-dispersive X-ray spectrometer. The accelerating voltage was 15 kV and the beam current varied between 3.5 and 5.5 nA. Bruker ESPRIT v2.5 software was used to process the EDS data post-acquisition.

Six electron transparent lamellae (hereafter referred to as FIB [focused ion beam] sections) were prepared, four from SAH 97072 and two from NWA 13299, using an FEI Helios Plasma Focused Ion Beam (P-FIB)-SEM0 instrument in the Kelvin Nanocharacterisation Centre (KNC) at the University of Glasgow, using a xenon plasma source following standard protocols (Lee et al.,

2003). These FIB sections were analyzed with scanning transmission electron microscopy (STEM) using JEOL ARM200CF and FEI TECNAI T20 instruments, also in the KNC at the University of Glasgow. The accelerating voltage used was 200 kV; samples were analyzed in both TEM and STEM mode. The FIB sections were additionally analyzed with SEM-EDS, and for transmission Kikuchi diffraction (TKD) using a Zeiss Sigma VP SEM equipped with a 170 mm^2 EDS detector and a Symmetry 2 electron backscatter diffraction (EBSD) detector from Oxford Instruments in the Geoanalytical Electron Microscopy and Spectroscopy (GEMS) center at the University of Glasgow, following the approach of (Trimby, 2012). The accelerating voltage was 20 kV and the beam current used was 4 nA. The step size for the TKD maps was 0.03–0.04 μm. EDS data were analyzed using Aztec software and TKD data were processed with the Aztec Crystal software from Oxford Instruments. TKD data were cleaned using a wildspike correction and a 6-point iterative nearest neighbor zero solution (Bestmann & Prior, 2003; Forman et al., 2016). Measured crystallographic data (i.e., Kikuchi diffraction patterns), paired with the crystallographic database in Aztec Crystal, allowed us to perform TKD indexing on phases in each FIB section in an attempt to identify phases.

Elemental Analyses

Elemental mapping was performed on areas adjacent to FIB section sites using laser ablation inductively coupled plasma–mass spectrometry (LA-ICP-MS) at the University of Manchester, using a Teledyne Photon Machine Analyte Excite+193 nm ArF excimer laser ablation system equipped with a HelEx II active 2-volume ablation cell, coupled to an Agilent 8900 ICP-MS. National Institute of Standards and Technology synthetic glass standard NIST 610 and 612 (Woodhead & Hergt, 2001), and the United States Geological Survey (USGS) basaltic glass standard BHVO-2G, BCR-2G, and BIR-1G (Elburg et al., 2005; Jochum et al., 2005b) were used for instrumental calibration and data quality control. Ablation of the NIST 612 glass was used to tune the ICP-MS, optimizing signal intensities while maintaining low levels of oxide formation ($^{232}ThO/^{232}Th = 0.3$) and a $^{238}U/^{232}Th$ ratio close to unity. For each map, the masses ^{23}Na (15 ms), ^{26}Mg (15 ms), ^{27}Al (15 ms), ^{29}Si (15 ms), ^{31}P (30 ms), ^{34}S (15 ms), ^{39}K (15 ms), ^{44}Ca (15 ms), ^{52}Cr (15 ms), ^{55}Mn (15 ms), ^{56}Fe (15 ms), ^{57}Fe (15 ms), ^{60}Ni (15 ms), ^{63}Cu (15 ms), and ^{66}Zn (15 ms) were analyzed (dwell times indicated in brackets), for a total of 0.2880 s per cycle. Mapped areas ranged in size from 246 × 200 μm^2 for SAH 97072 to 196 × 200 μm^2 for NWA 13299, and maps were collected by stacking individual LA-ICP-MS line analyses. We used a 5 μm^2 laser spot, a 10 Hz repetition rate, 5 J cm^{-2} fluence, 5 μm vertical distance between lines, and a laser scan speed of 5 μm s^{-1}. This resulted in a spatial resolution per pixel of 1.44 μm in x and 5 μm in y. After each laser line, there was a pause of 15 s during which background counts for the masses of interest were integrated.

The raw LA-ICP-MS map data were processed using the Iolite 4 software (Paton et al., 2011). Element intensity maps were first constructed using the 'Imaging' function of Iolite. Regions of interest (ROI) corresponding to the different phases of interest were then defined manually. Average element concentrations and standard deviations were calculated for each ROI. To calculate element abundances in these phases, we used the 'Trace Elements' data reduction scheme of Iolite, using known Fe abundances for reference materials (Jochum, Nohl, et al., 2005), and the approximate Fe abundances of 50 wt% for djerfisherite (Clay et al., 2014) and 63 wt% for QR areas (based on the Fe abundance of troilite; El Goresy et al., 1988). The reference glasses were analyzed using the same setup before and after each map, and at regular intervals during the analysis of each mapped section. BHVO-2G was used as the primary reference material, and NIST 610, BCR-2G, and BIR-1G were treated as unknowns and used as quality control reference materials. For all the elements analyzed, accuracy was typically within ±20% of recommended values except for low abundance elements such as P in BIR-1G and Cr in BCR-2G (see File S1).

RESULTS

The Presence or Absence of the Qingzhen Reaction in Djerfisherite-Bearing Meteorites

We first compare various features of meteorites containing djerfisherite, in order to highlight similarities and differences in factors such as shock and weathering, between those that do and do not contain the QR. Table 1 summarizes key properties of djerfisherite-bearing EH chondrites, with and without the QR, as well as djerfisherite-bearing EL3 and djerfisherite-bearing aubrites. As seen in Table 1, the QR is only present in some EH3: We observed it in 6 of the 11 djerfisherite-bearing EH3 samples studied. There is no apparent reason why some EH3 show the QR and others do not, and no other mineralogical differences are obvious between these two categories (Mc Ardle et al., 2025). The QR has never been observed in any other djerfisherite-bearing meteorite types, including in the EL3 chondrites and aubrites (Table 1). The shock grades of both EH3-QRB and EH3-nonQRB are S2–S3, with the exception of the EH3-QRB Y-691 which is S4. All the

EH3-nonQRB samples are finds from Antarctica, while the EH3-QRB include a fall (Qingzhen) and finds from both hot and cold deserts. The weathering grade of the EH3-nonQRB varies from W1 to W3 while the weathering grade of EH3-QRB varies from W0 to W1. In addition, none of the djerfisherite-bearing EL3 chondrites or aubrites exhibit the QR, irrespective of whether the meteorite is a fall versus find or its weathering grade.

Mineral Associations of Djerfisherite and the Qingzhen Reaction in EH3 chondrites

Since the QR is confined to EH3 chondrites, we focus on these samples to investigate the mineralogical associations of djerfisherite, and the petrologic context of the QR. In the EH3, djerfisherite occurs in three contrasting mineralogical associations (Figure 2). The first association is within complex, often layered, polyphase MSN (Figure 2a,b). MSN is commonly comprised of a wide range of sulfides (djerfisherite, niningerite/alabandite, daubréelite, troilite, sphalerite, and oldhamite), as well as metal, schreibersite, perryite, silicates (enstatite, silica, feldspar, and roedderite), and silicate glass (Jacquet et al., 2018; Lehner et al., 2013; Weisberg & Kimura, 2012). When djerfisherite occurs in MSN it can be located toward the center or closer to the edge of the nodule. Other phases within the MSN occasionally occur as inclusions within djerfisherite. There appears to be no preference for which minerals are in contact with the djerfisherite. The second association is solitary djerfisherite occurring outside of MSN, within the matrix of the meteorites (Figure 2c,d). These djerfisherite occurrences can range from <5 μm to several hundred micrometers in diameter. Both the MSN and solitary djerfisherite mineral associations are common in the EH3. The third mineral association of djerfisherite in the EH3 chondrites is within veins, both mono- and polyphase, in the case of the latter along with, for example, metal, troilite, oldhamite, and niningerite/alabandite. This association is rarer and only occurs in some EH3. In the studied samples, both MIL 07028 (EH3-nonQRB) and NWA 13299 (EH3-QRB) contain rare metal and sulfide veins, including mono- and polyphase djerfisherite grains (Figure 2e,f). These veins are elongate with spidery webs of subordinate veins which appear to feed into or off a larger vein (Figure 2e, f). In two of the four samples of MIL 07028 which we analyzed, we observed relatively abundant djerfisherite, along with other phases (metal, troilite, niningerite, and daubréelite) in veins that can extend several hundred micrometers across the sample (a relatively small example is shown in Figure 2e). Our sample of NWA 13299 contains an extended vein network in one part of the section, dominated by troilite and djerfisherite, along with other phases (e.g., metal, daubréelite). We note that the sections we have viewed are two-dimensional, and that in three dimensions the solitary djerfisherite occurrences could be MSN which coincidentally only constituted djerfisherite at the polished surface. It is not impossible that in some cases the solitary djerfisherite grains are also discrete veins cut approximately perpendicular to their elongated direction. However, we think this latter scenario is very unlikely as the veins which we observed are rarely simple discrete objects and instead comprise a complex vein network, none of which we see associated with any of the solitary djerfisherite. Djerfisherite was never found within chondrules of any of the studied meteorites, which agrees with the observations of Clay et al. (2014); Ebel and Sack (2013). However, there are a few instances where djerfisherite partially surrounds the exterior of chondrule rims either as solitary djerfisherite or in what appears to be deformed MSN.

Importantly, when the QR occurs in a sample, every mineralogical association of djerfisherite exhibits the QR, including the veins, as shown in Figure 2. The one known exception is djerfisherite grains entirely enclosed by metal, described by Lin and El Goresy (2002); however, we did not observe such occurrences of djerfisherite in any of the samples studied here.

LA-ICP-MS Geochemical Maps

It is clear from SEM-EDS maps that the QR contains both Fe and S (Figure 1), corresponding to the presence of troilite as noted in previous studies (Lin & El Goresy, 2002). We obtained quantitative LA-ICP-MS maps in order to compare abundances of K, Na, Cu, and Ni in the djerfisherite and the QR. The aim here was to assess the fate of these djerfisherite components, and to test whether there were any Zn hotspots in the QR, which could indicate the presence of sphalerite. We note that djerfisherite also contains 1.5 wt% Cl (Clay et al., 2014). However, since reliable Cl analyses were not possible on the LA-ICP-MS, we did not attempt to quantify this element. LA-ICP-MS maps were obtained on a portion of a QR-bearing solitary djerfisherite grain within SAH 97072 (Figure 3) and on a portion of QR-bearing djerfisherite in a polyphase vein in NWA 13299 (Figure 4).

Djerfisherite is clearly defined in Figures 3 and 4 by comparatively high abundances of K, Cu, and Ni. In contrast, the QR has lower K, Cu, and Ni abundances, but somewhat higher Na abundances. Any hotspots of K, Cu, and Ni found within the QR coincide with each other, indicating that these hotspots are likely to be remnant djerfisherite (Figures 3b,d,e and 4b,d,e). No standalone K or Cu hotspots were found. The Zn maps

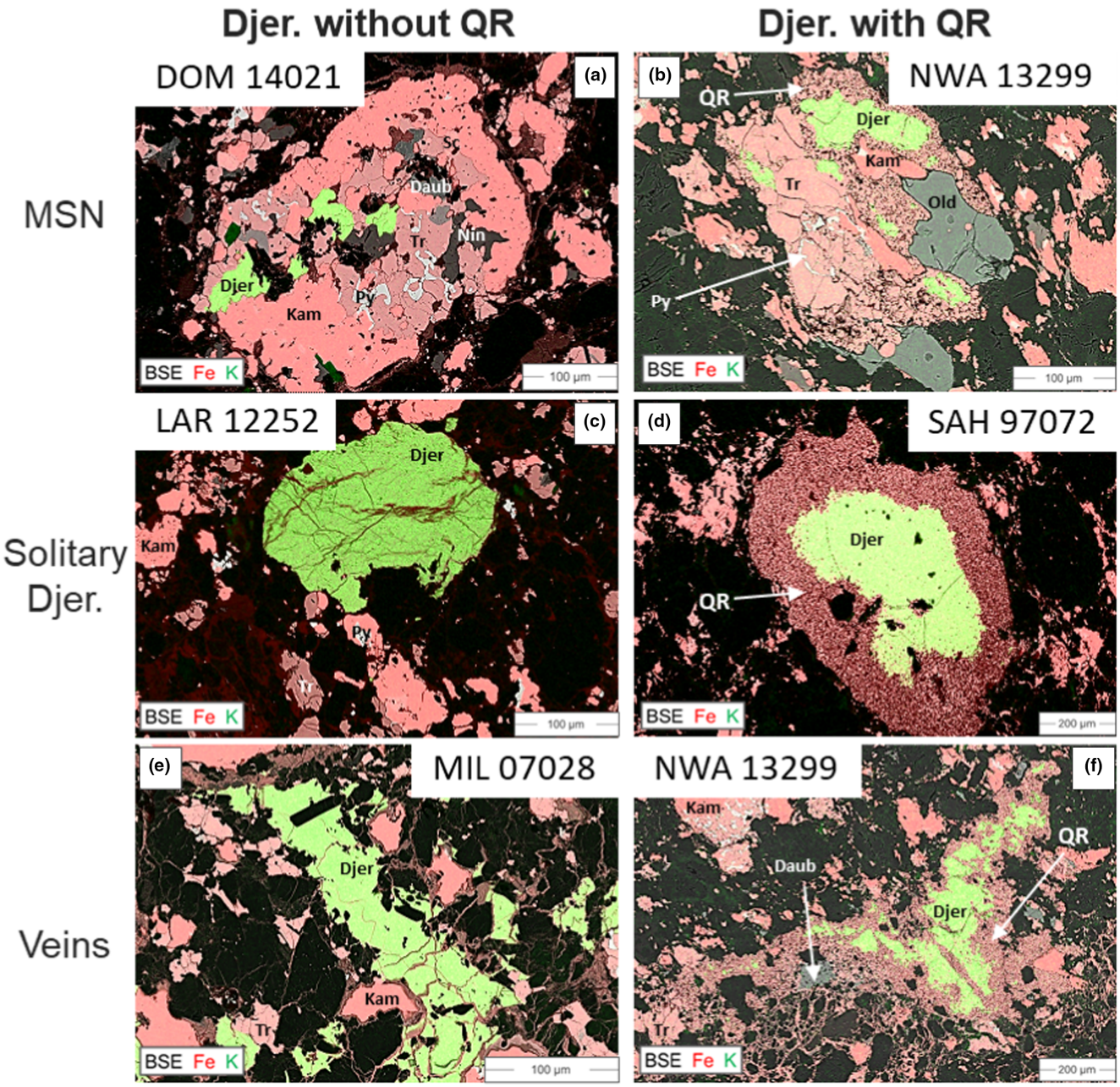

FIGURE 2. Composite BSE (gray) and SEM-EDS maps (Fe red, K green) of djerfisherite in various EH3. Djerfisherite (Djer) is shown in green, and red colors show metal (Kam; deepest red) and troilite (medium red). Mineral associations noted on left are as follows: (a, b) polyphase MSN, (c, d) solitary djerfisherite within matrix, and (e, f) Poly/mono-phase veins. Djerfisherite in LAR 12252 (c) and MIL 07028 (e) exhibits some interior Fe-rich weathering veins. Panels on the left (a, c, e) do not show the Qingzhen reaction (QR), and panels on the right (b, d, f) show the QR as a fine-grained, porous, Fe-rich assemblage surrounding djerfisherite (labeled QR). Notes on other minerals: phases appearing black are silicates/glass (mostly enstatite), the phases appearing gray (a, b, and f) are niningerite (Nin) daubréelite (Daub) and oldhamite (Old), the phase appearing white/light gray/light pink (i.e., stringy phase within MSN in a, b, c and upper left of f) is perryite (Py). Schreibersite (Sc) is also present (e.g., a) appearing as the phase with an intermediate red (i.e., intermediate between kamacite and troilite). Note that in b, large grains of oldhamite are directly juxtaposed against the QR.

(Figures 3f and 4f) show a few small Zn hotspots a few micrometers across within the QR across both samples (note two larger Zn hotspots occur within the matrix of SAH 97072 in Figure 3f), possibly indicating the presence of small sphalerite grains. Element abundances calculated for djerfisherite and QR regions of interest (ROI) are

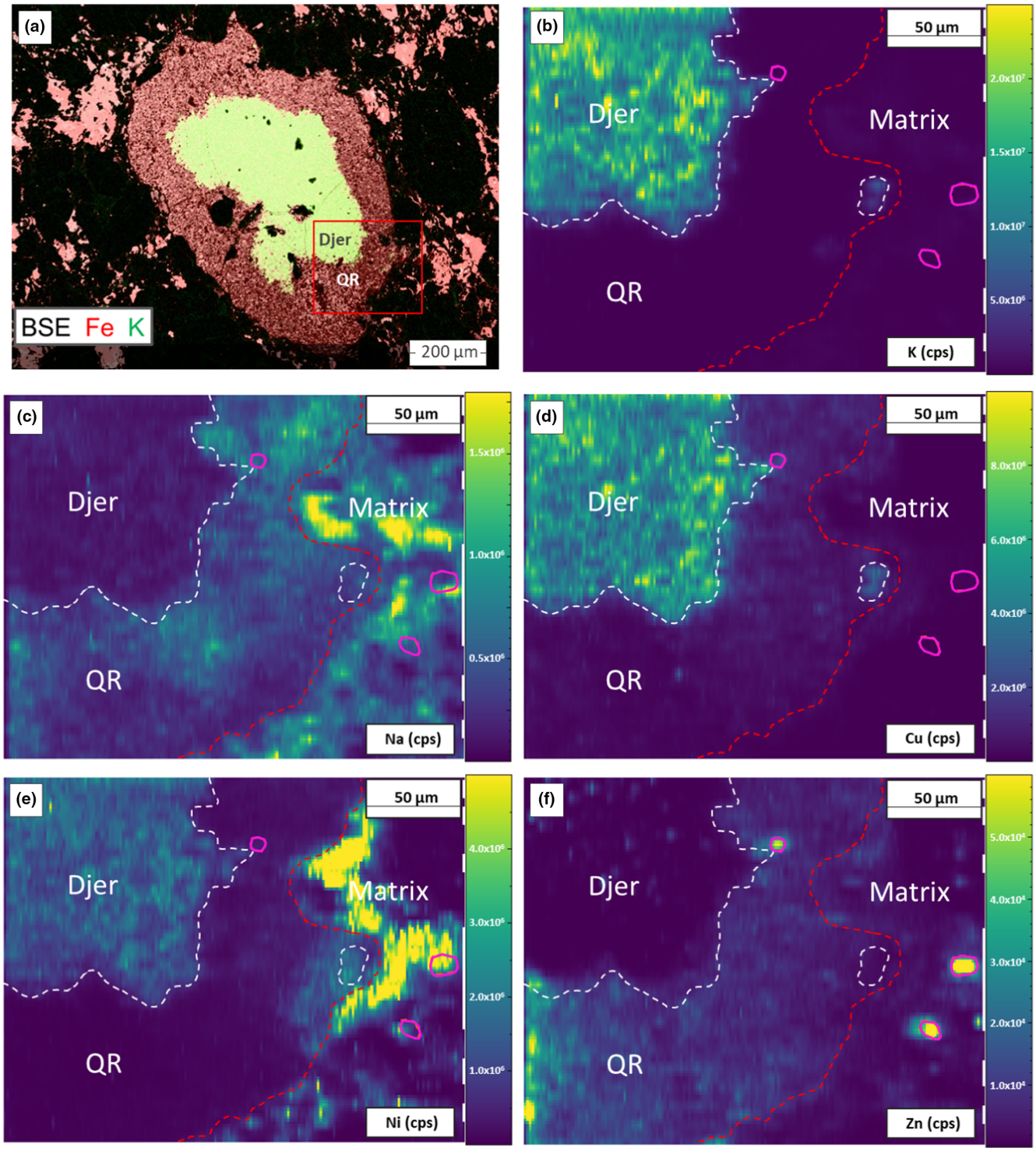

FIGURE 3. Elemental distributions in a solitary djerfisherite with associated QR occurrence in SAH 97072. (a) Composite BSE (gray) and SEM-EDS maps (Fe red, K green) showing djerfisherite (Djer) in green and the Qingzhen Reaction (QR) in red. (b–f) Quantitative LA-ICP-MS intensity maps for K, Na, Cu, Ni, and Zn of the area indicated with a red box in (a), showing unaltered djerfisherite (within white dashed lines), QR (between white and red dashed lines), and sphalerite (within solid magenta line). Note, placement of the red dashed line, separating the QR and the matrix was partially based on other element maps, not shown here, for example, Si and Fe.

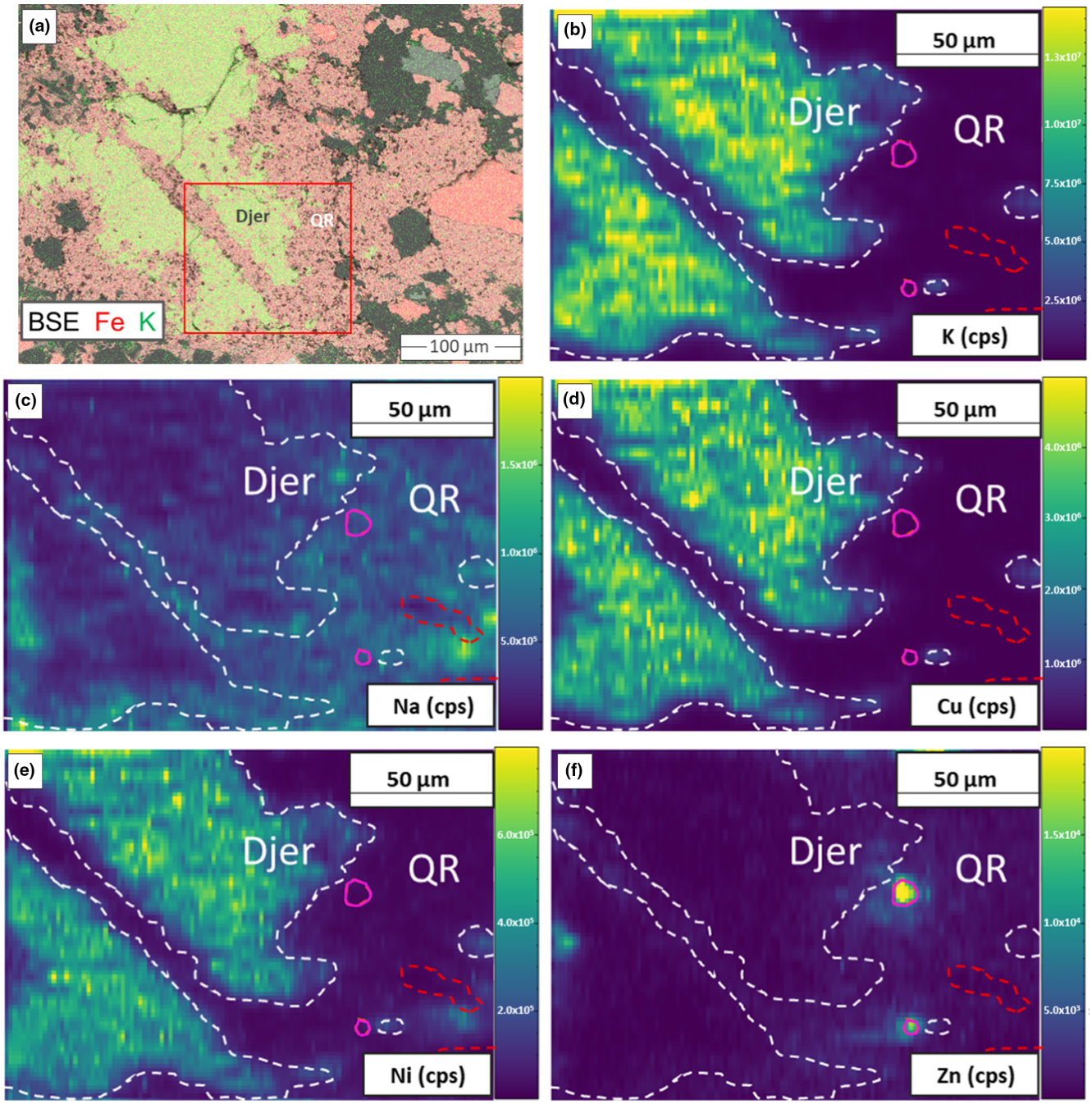

FIGURE 4. Elemental distributions in a polyphase vein in NWA 13299 showing djerfisherite with associated QR. (a) Composite BSE (gray) and SEM-EDS maps (Fe red, K green) showing djerfisherite (Djer) in green and Qingzhen Reaction (QR) in red. (b–f) Quantitative LA-ICP-MS intensity maps for K, Na, Cu, Ni, and Zn of the area indicated with a red box in (a), showing unaltered djerfisherite (within white dashed lines), QR (between white and red dashed lines), and sphalerite (within solid magenta line). Note, placement of the red dashed line, separating the QR and the matrix was partially based on other element maps, not shown here, for example, Si and Fe.

reported in Table 2. In both SAH 97072 and NWA 13299, calculated K abundances in the djerfisherite (71,132 and 81,152 µg g^{-1}, respectively) are significantly higher than in the QR (501 and 6202 µg g^{-1}, respectively). In both SAH 97072 and NWA13299, Na abundances are lower in djerfisherite (745 and 2350 µg g^{-1}, respectively) than in the QR (3072 and 11,272 µg g^{-1}, respectively), while Cu and Ni

concentrations are about an order of magnitude higher in the djerfisherite (30,781 and 30,998 μg g^{-1} for Cu and 21,996 and 10,382 μg g^{-1} for Ni, respectively) compared to the QR (3803 and 2172 μg g^{-1} for Cu and 3260 and 2148 μg g^{-1} for Ni, respectively). Zn abundances are similarly low in djerfisherite (12 and 9 μg g^{-1} in SAH 97072 and NWA13299, respectively) and the QR (321 and 170 μg g^{-1}, respectively) in both samples.

Mineralogy and Microstructure of the Qingzhen Reaction

We prepared four FIB sections from SAH 97072, all from the same QR-bearing solitary djerfisherite grain as that analyzed by LA-ICP-MS (Figures 5a,b and 6a–d). FIB1 and FIB2 were located on the interior of the QR, covering the QR-djerfisherite boundary. FIB3 was located at the external boundary of the QR where the QR is juxtaposed against an enstatite grain. FIB6 is located in the middle of the QR. In NWA 13299, we prepared two FIB sections, both from QR-bearing djerfisherite in a MSN (Figures 5c,d and 6e,f). FIB4 is located at the exterior boundary of the QR where the QR is juxtaposed against a kamacite grain. FIB5 is located at the interior boundary of the QR, covering the QR-djerfisherite boundary.

This range of placement of FIB locations in both samples was aimed at determining whether there is any variability between interior, central, and exterior parts of the QR. We found that all six FIB sections are very similar, in terms of the textural and mineralogic characteristics of the QR and djerfisherite (if present). Therefore, in the remainder of the paper, we focus on two specific FIB sections, FIB1 from SAH 97072 and FIB5 from NWA 13299, both of which cover the djerfisherite-QR boundary.

SEM-EDS and TKD results from all FIB sections are very similar. They show that the QR is comprised of up to four different phases along with pore space (Figure 7). Two phases typically exhibit high band contrast (a measure of Kikuchi pattern quality) and were successfully indexed via TKD: troilite and djerfisherite. SEM-EDS maps confirm that the dominant mineral phase in the QR (shown in green in the SEM-EDS maps of Figure 7) contains Fe and S as major elements, and very little else detectable by SEM-EDS. TKD indexing confirms that this phase is troilite. SEM-EDS maps also indicate the presence of a phase containing K, S, and Fe (shown in yellow/brown in the SEM-EDS maps of Figure 7), which TKD confirmed to be djerfisherite. In addition to occurring outside of the QR as unaltered djerfisherite, djerfisherite also occurs within the QR as small, isolated grains associated with troilite, hereafter referred to as remnant djerfisherite. Inverse pole figure maps indicate that the troilite grains in the QR in NWA 13299 are not single crystals, but instead they are comprised of interlocked crystals with apparent dihedral angles all approaching 120° at triple junctions (Figure 7b). This is also true for the troilite within SAH 97072 (Figure 7d); however, it is less apparent in this sample due to less successful indexing of the troilite. Unaltered djerfisherite in NWA 13299 appears to be a single crystal (Figure 7b). Remnant djerfisherite "islands" within the QR have different crystallographic orientations to the main djerfisherite grain. In contrast, djerfisherite within SAH 97072 is polycrystalline (Figure 7d).

The two other phases that were found, but not indexed due to the phases not yielding indexable Kikuchi patterns, are an Fe-O bearing phase in both samples (shown in blue in the SEM-EDS maps of Figure 7) and Na- and Cl-bearing hotspots in SAH 97072 (shown in red in the SEM-EDS maps of Figure 7).

We used transmission electron microscopy (TEM) in order to determine the nature of the Fe-O bearing phase observed in QR regions. This phase has a fibrous habit and appears to rim the pores and in places to bridge pore

TABLE 2. Selected element abundances for djerfisherite and the QR in SAH 97072 and NWA 13299, obtained from LA-ICP-MS maps.

	K		Na		Fe		Ni		Cu		Zn	
	Ave. μg g^{-1}	StDev. μg g^{-1}	Ave. μg g^{-1}	StDev. μg g^{-1}	Ave. μg g^{-1}	StDev. μg g^{-1}	Ave. μg g^{-1}	StDev. μg g^{-1}	Ave. μg g^{-1}	StDev. μg g^{-1}	Ave. μg g^{-1}	StDev. μg g^{-1}
SAH 97072												
Djer	71,133	2420	745	16	494,692	13,316	21,996	881	30,781	843	12	7
QR	501	38	3072	470	626,505	14,085	3260	3509	3803	1372	321	176
NWA 13299												
Djer	81,152	2800	2350	411	473,945	3275	10,382	11	30,998	331	9	2
QR	6202	4442	11,272	1314	632,346	1356	2148	997	2172	1207	170	59

Note: Averages are mean values across two regions per sample for djerfisherite, two regions for NWA 13299 QR, and three regions for SAH 97072 QR.

Abbreviations: Ave -average; Djer - djerfisherite; QR - Qingzhen Reaction; St.Dev - 1 sigma standard deviation of the mean.

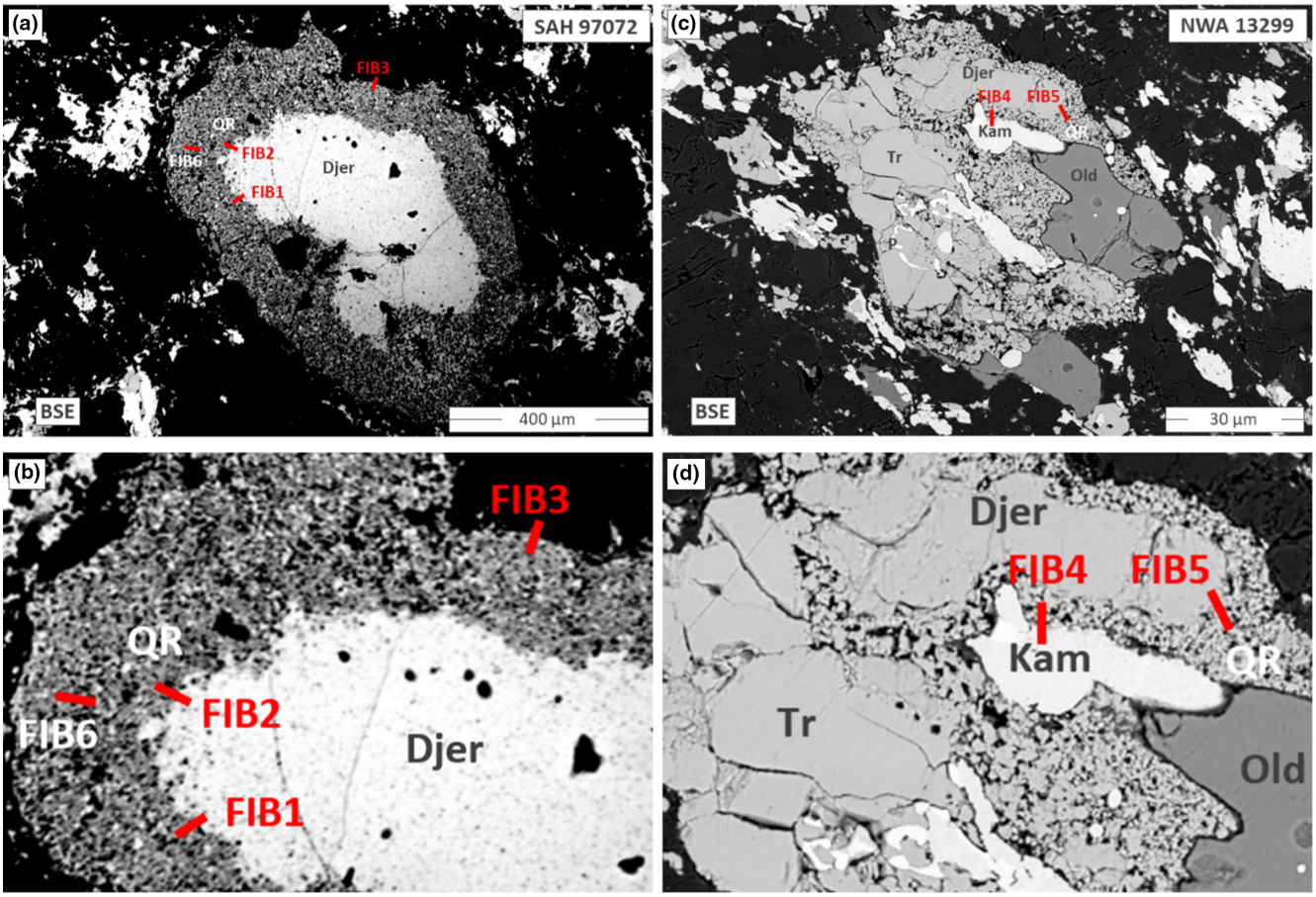

FIGURE 5. BSE maps of (a, b) solitary djerfisherite in SAH 97072 and (c, d) a djerfisherite-bearing MSN in NWA 13299, showing FIB section locations. (b) and (d) Enlarged versions of (a) and (c). Note the direct juxtaposition of oldhamite against the QR in (d).

throats (Figure 8). Attempts were made to examine the atomic spacing within this phase, in order to determine its microstructure. However, this was hampered by the fine-grained nature of this phase, in addition to its apparent susceptibility to beam damage. As such, a positive mineral identification was not possible. We suggest that it may be an oxide or a hydroxide. We note that the Fe-O phase is actually evident in Figure 1b, located between troilite grains in the QR; it has a brighter/deeper shade of red than that of the troilite.

The Na- and Cl-rich phase that occurs in the interior of some troilite grains was found only in SAH 97072 in some FIB sections. Although we could not identify this phase with TKD indexing, we suggest it is halite. We did not observe any additional phases within either the QR or the djerfisherite, despite a concerted effort to find covellite, bornite, idaite, sphalerite, and various Fe-O bearing phases (e.g., magnetite, goethite, etc.) by means of TKD indexing and SEM-EDS observation. Some individual pores extend a considerable distance within the QR (e.g., the annotated pore in FIB6 which extends for at least 6 µm; Figure 6d). There appears to be a slightly higher proportion of pore space in the QR of SAH 97072 compared to NWA 13299 (Figure 7).

DISCUSSION

Origin of Djerfisherite

Based on our observations, we conclude that the majority of djerfisherite in the EH3, particularly the djerfisherite within MSN, formed prior to accretion, either as a direct condensate from the nebula (Clay et al., 2014; Ebel & Sack, 2013) or through sulfidization of metal in the nebula (El Goresy et al., 1988; Lin & El Goresy, 2002). We believe this is the best interpretation of the complex, layered texture of these MSNs. We also interpret solitary djerfisherite grains within the matrix as having formed prior to accretion, as they exhibit no vein-like characteristics and have textures that indicate they accreted coevally with the surrounding material. However, it is possible that in some cases, solitary

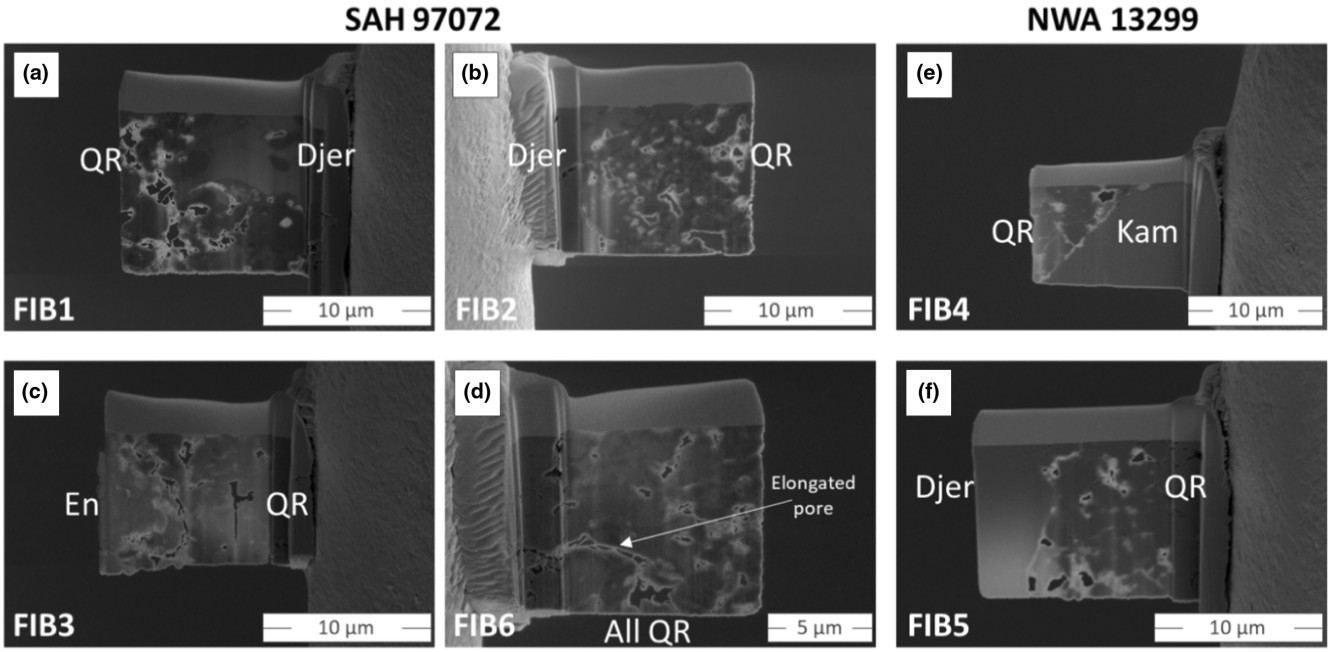

FIGURE 6. Secondary electron (SE) images of FIB sections in SAH 97072 (a–d) and NWA 13299 (e, f). Long QR pore in FIB6. Djer - djerfisherite; En - enstatite; Kam - kamacite; QR - Qingzhen reaction.

djerfisherite grains could be either MSN or (in our view less likely) veins that have been cut in the transverse plane.

We disagree with the argument of El Goresy et al. (1988); Lin and El Goresy (2002) that opaque veins (occasionally djerfisherite-bearing) within the Qingzhen meteorite (or other EH3) are pre-accretionary. Opaque veins in the ECs have complicated textures (see Figure 2e, f), which we argue indicate that they formed through the injection/percolation of liquified and/or vapor metal and sulfide phases into pre-accreted material, for example, injection into fractures. We prefer the explanation that these veins formed post-accretion as a result of mobilization of existing sulfides in response to shock (Rubin, 2015). We observed veins in both the EH3-nonQRB MIL 07028 and the EH3-QRB NWA 13299, while El Goresy et al. (1988) and Lin and El Goresy (2002) reported similar veins in EH3-QRB Qingzhen. All three of these meteorites have a shock stage of S3: indeed, in support of this argument, Rubin (2015) identified opaque shock veins as a feature of S3 ECs.

What Does the Presence or Absence of the Qingzhen Reaction Tell Us?

Despite the presence of djerfisherite in other meteorite types (e.g., some EL3, aubrites), the QR is only present in some EH3. Therefore, we conclude that the QR is restricted to the EH parent body. Since not all EH3 chondrites exhibit the QR, the reaction was either limited spatially within a single parent body, or there were multiple EH parent bodies that experienced different conditions.

If shock process were responsible for the development of the QR we would expect to see a correlation between the presence/absence of the QR and shock (i.e., EH3 with higher shock stages would have greater incidence of the QR). However, we do not observe this; EH3-nonQRB and EH3-QRB have similar shock stages of S2–S3. Additionally, if shock alone was responsible for the QR, we could expect djerfisherite in other types of meteorites (e.g., EL3, aubrite) to exhibit the QR, which is not observed. Therefore, we conclude that shock processes are not directly responsible for the formation of the QR.

If the QR formed on Earth due to terrestrial alteration, we would expect to see a correlation between the presence/absence of the QR and the degree of weathering (i.e., more weathered samples would have more QR). In this study, all of the EH3-nonQRB samples are finds from Antarctica, while the EH3-QRB includes a fall (Qingzhen) but are mainly finds from both hot and cold deserts. The weathering grades of the EH3-nonQRB vary from W1 to W3, while the weathering grade of EH3-QRB varies from W0 to W1. Therefore, we conclude there is no correlation between the presence/absence of the QR

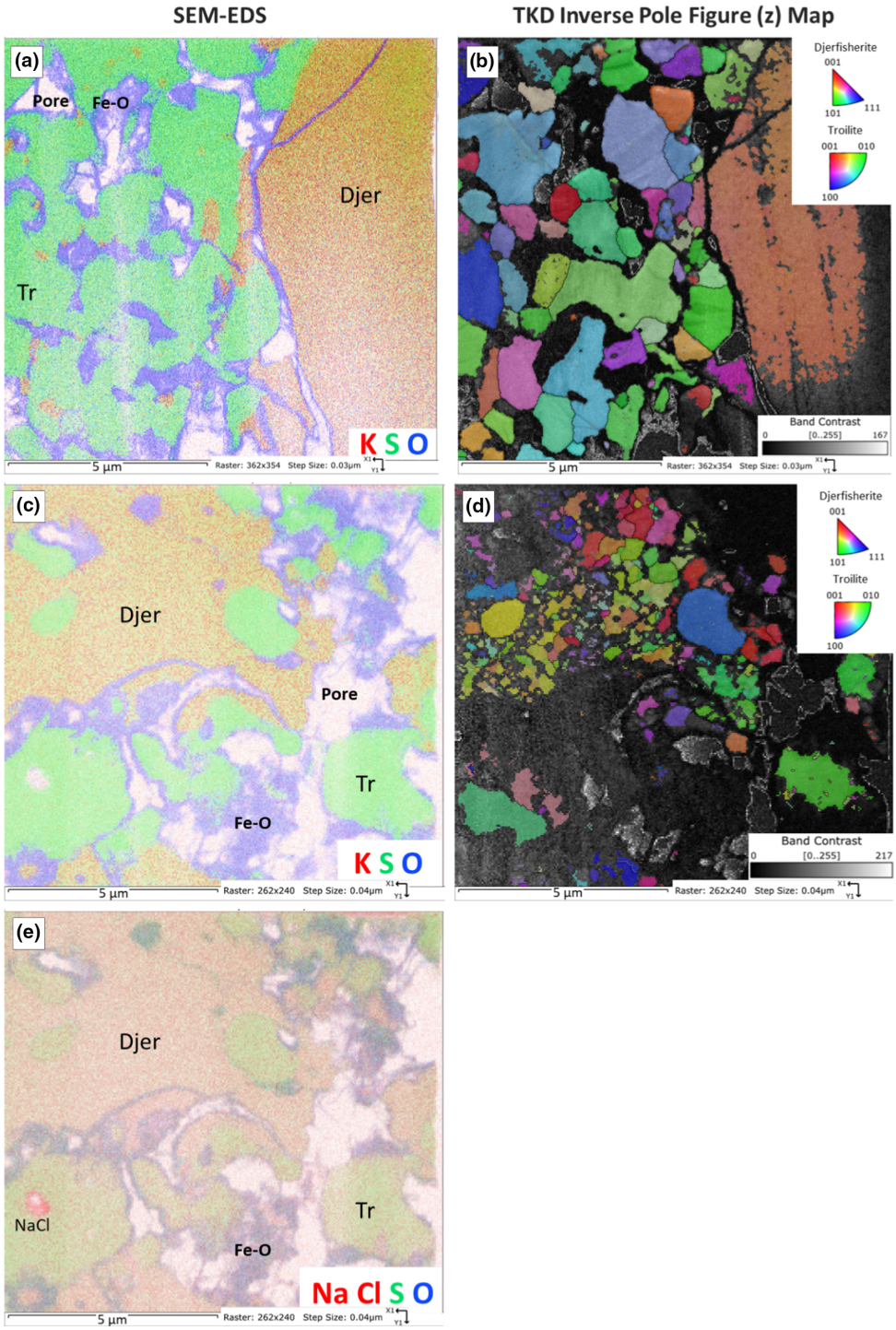

FIGURE 7. (a, c, e) SEM-EDS maps (K red, S green, O blue, and Na and Cl red) and (b, d) TKD inverse pole figures with band contrast. (a, b) NWA 13299 FIB5, (c–e) SAH 97072 FIB1. Djer - djerfisherite; Fe-O - fibrous Fe-O bearing phase; Tr - troilite.

and fall/find location or degree of weathering, indicating that terrestrial weathering is not a causal factor in QR formation.

Geochemistry and Mineralogy of the QR

Based on our petrographic, geochemical, and mineralogical observations and as proposed by El

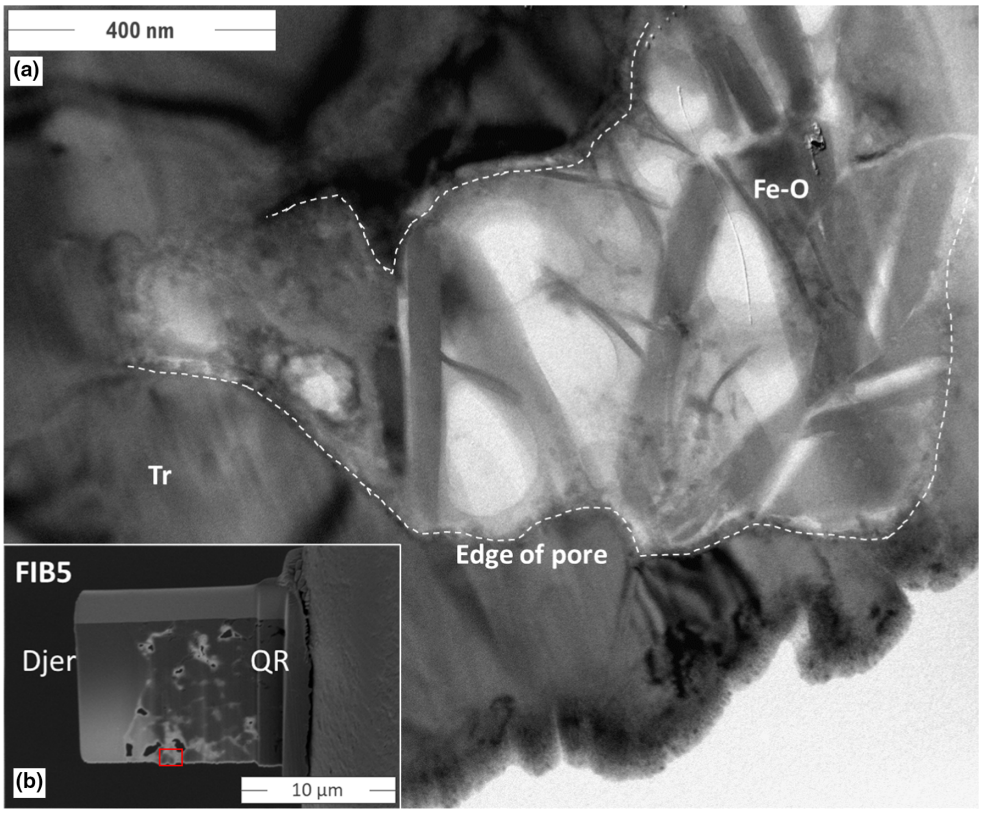

FIGURE 8. (a) TEM bright-field image of a region of QR region in NWA 13299 FIB5. The fibrous Fe-O-rich phase partially fills pore space between troilite grains. (b) SEM SE image of entire FIB5 showing location of image A in the red box. Fe-O - fibrous Fe-O bearing phase; Djer - djerfisherite; QR - Qingzhen reaction; Tr troilite.

Goresy (1985), El Goresy et al. (1988), Lin and El Goresy (2002), we interpret the QR as an alteration, a "breakdown," of djerfisherite. Our geochemical analyses allow us to examine the elemental loss and gain as a result of this alteration, which assists in better defining the nature of the reaction.

Geochemical analyses obtained via LA-ICP-MS show similar results for both SAH 97072 and NWA 13299. It is clear that the majority (92%–99%) of the K in the djerfisherite was lost during the formation of the QR (Table 2). We suggest that any remaining K is largely sited in islands of remnant djerfisherite within the QR, such as those illustrated in Figures 3b and 4b and 7, and that the slightly higher K concentration in the QR of NWA 13299 might reflect a relatively higher abundance of remnant djerfisherite in the area studied. Although Na concentrations are low in both the djerfisherite and the QR, concentrations are 75%–79% higher in the QR. We know that remnant djerfisherite and the Na-Cl hotspots will contain some Na within the QR. However, these cannot account for all of the observed Na in the QR. Therefore, we can only conclude that the bulk of the Na is sited in troilite, and/or associated with the fibrous Fe, O-bearing phase. The majority of Cu (88%–93%) and Ni (79%–85%) were lost from djerfisherite during the formation of the QR, with the remaining Cu and Ni in the QR likely sited in remnant djerfisherite and/or troilite. The Zn concentration is low in both the djerfisherite and the QR; however, there is a slightly higher concentration in the QR which overall represents a 95%–98% increase. Several Zn hotspots a few micrometers in size were found within the QR of both SAH 97072 and NWA 13299. We interpret this as sphalerite, although we cannot rule out the possibility that this is another polymorph in the Zn-Fe-S system. Given that sphalerite in the QR was neither detected in any of the FIB sections, nor in our SEM-EDS mapping of the samples, we conclude that these grains are extremely rare, that is, present in trace abundances only.

In addition, Figure 7e shows the presence of Na- and Cl-bearing hotspots that are located within troilite. We suggest that these are halite, although this could not be confirmed by TKD indexing as the region did not yield Kikuchi patterns. The presence of halite within troilite grains suggests that halite is indigenous to the host chondrite, and formed at the time of the QR. If these halite grains were a terrestrial weathering product, we might have expected them to be situated within the QR pores, which they are not. The presence of the halite

within troilite grains may have protected them from incipient terrestrial weathering (as indicated by the Fe-O phase, see below).

We interpret the fibrous Fe-O bearing phase which is found in the pores of the QR as an unidentified terrestrial weathering product. A meteoritical Fe-O bearing phase within the ECs is unlikely due to their highly reduced nature. Since the ECs generally have low porosity (Macke et al., 2010), we suggest that despite the low weathering grade of both SAH 97072 and NWA 13299, the highly porous nature of the QR in particular makes it susceptible to some terrestrial alteration.

The lack of standalone K hotspots in the QR indicates that there is no evidence for the presence of the "unknown K-bearing mineral" of El Goresy et al. (1988). The K hotspots coincide with Cu and Ni hotspots (Figures 3 and 4), indicating these are remnant djerfisherite within the QR. This is backed up by the SEM-EDS and TKD images of FIB sections (Figure 7), where no additional K-bearing minerals are observed, but remnant djerfisherite is common. Therefore, we suggest the "unknown K-bearing mineral" of El Goresy et al. (1988) may be remnant djerfisherite.

The lack of standalone Cu hotspots also indicates that there is no evidence for the Cu-bearing sulfides (covelline, bornite, and idaite) found by El Goresy et al. (1988), and Lin and El Goresy (2002). This is confirmed by the SEM-EDS and TKD of FIB sections in which we did neither identify any covellite, bornite, nor idaite (Figure 7). El Goresy et al. (1988) suggested that Cu-bearing sulfides formed due to the release of Cu from djerfisherite during the formation of the QR. However, covellite and bornite are known weathering products of meteorites (Erokhin et al., 2018; Rubin, 1997) and covellite, bornite, and idaite are known weathering products of terrestrial ore deposits (Wang et al., 2014). These phases were initially only found in the moderately weathered Antarctic find Y-691 (El Goresy et al., 1988). Later, Lin and El Goresy (2002) reported their presence in Qingzhen. Although Qingzhen is a fall, some fragments were recovered up to 2 weeks after it fell (Meteoritical Bulletin, accessed June 12, 2024), and a sample of Qingzhen that we analyzed has a weathering grade of W1 (Table 1). Also, the observations in Lin and El Goresy (2002) were made 26 years after Qingzhen fell. Given their reduced nature, ECs are particularly susceptible to terrestrial weathering, and it is likely that terrestrial weathering of Qingzhen developed either pre-recovery or while in storage in collections, or both. For these reasons, we argue that covellite, idaite, and bornite described by El Goresy et al. (1988), and Lin and El Goresy (2002) in the QR of Y-691 and Qingzhen are likely terrestrial weathering products.

We observed very rare occurrences of sphalerite within the QR (Figures 3f and 4f), and it has previously been inferred that this is a product of the QR reaction (El Goresy et al., 1988; El Goresy & Ehlers, 1989). This poses a conundrum because djerfisherite contains almost no Zn (Table 2). El Goresy and Ehlers (1989) and El Goresy et al. (1988) reported porous/frothy sphalerite associated with the QR in both Qingzhen and Y-691. They took the porous/frothy nature of the sphalerite to indicate it was associated with the QR because the QR troilite was also porous/frothy. However, El Goresy and Ehlers (1989) also reported porous/frothy sphalerite within the EH4 Indarch, which does not appear to contain djerfisherite: no djerfisherite is reported in the literature, and we found none in the Indarch samples analyzed in a related study (Mc Ardle et al., 2025). Therefore, Indarch does not contain the QR, and the proposed co-genetic association between porous/frothy sphalerite and the porous troilite comprising the QR (El Goresy et al., 1988; El Goresy & Ehlers, 1989) may be misleading. As an alternative suggestion to the sphalerite being formed through the QR reaction, we suggest the sphalerite could have originally occurred as inclusions in the precursor djerfisherite. The co-occurrence of djerfisherite and sphalerite is common in the MSN of the EH3. Due to the small nature of the sphalerite in the QR and its rarity, it has not been possible to examine it further in this study.

El Goresy and Ehlers (1989) and El Goresy et al. (1988) attempted to determine the temperature of formation of the QR. On the basis of the assumption that both covellite and idaite were formed by the QR, these authors used the stability fields of covellite and idaite to derive a temperature of formation for the QR of <780 K. They also examined sphalerite closure temperatures, based on the Fe content between co-occurring sphalerite and troilite pairs, and obtained temperatures of 650–732 K for Qingzhen, and 639–728 K for Y-691. However, assuming that the Cu-bearing sulfides are products of terrestrial weathering, and since the sphalerite may not be co-genetic with the QR, this approach is questionable. We therefore suggest that the temperature data derived from the Cu-sulfides should be discarded and that the sphalerite-derived temperature data should be treated with caution. There is currently no alternative way to estimate the temperature of QR formation.

In summary, troilite formed as the main *in situ* product of the QR at the expense of djerfisherite. Rare halite grains, observed as inclusions in troilite, formed contemporaneously. Extremely rare and small sphalerite grains may also have formed in the QR, but alternatively they may also have been present as inclusions within the precursor djerfisherite. Remnant djerfisherite, not transformed during the QR reaction, remained as

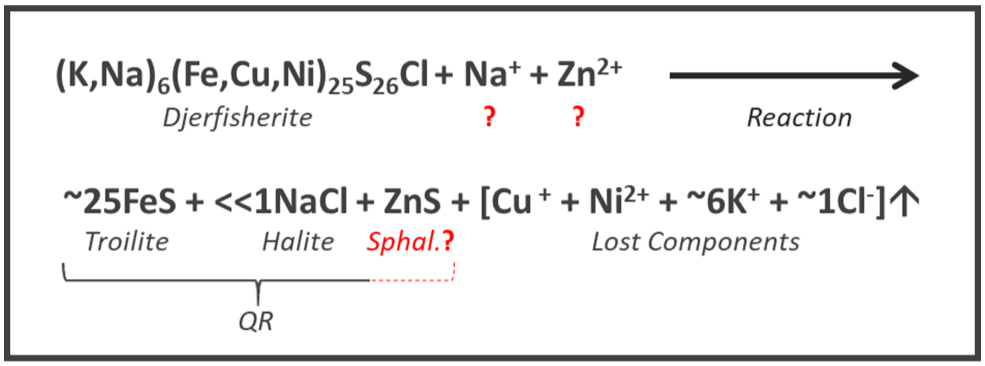

FIGURE 9. Approximate chemical reaction for the formation of the QR at the expense of djerfisherite. Components denoted in red are uncertain and may or may not take part in the reaction. Sphal, sphalerite. Reaction products formed *in situ* include the QR assemblage; djerfisherite components lost from the QR are denoted by the upward arrow.

"islands" in the newly formed QR. Figure 9 represents an approximate chemical reaction, including the products formed *in situ* and djerfisherite components lost from the QR (denoted by upward arrow).

Evidently Fe, S, Na, and a minor amount of Cl were retained in the QR after the breakdown of djerfisherite. However, the precursor djerfisherite lost the majority of its K, Cu, and Ni. Although we did not measure Cl abundances, we expect that the initial Cl content of djerfisherite is 1.5 wt% based on Clay et al. (2014). Therefore, it appears that most of the Cl was also lost, as the proportion of halite found in the QR is very low. The fate of these lost components from the QR is currently unknown. We suggest that they either diffused into surrounding components of the chondrite (e.g., matrix and chondrules), away from the djerfisherite and newly formed QR, or that they were lost from the system entirely. For Na, the slightly higher Na content of the QR compared to djerfisherite (Table 2) suggests the introduction of a small amount of Na as a reactant, although the siting of this additional Na in the QR is unclear. Perhaps the Na is sited in troilite, having been introduced in limited quantities during the formation of the QR. Alternatively, if the additional Na is sited in the fibrous Fe-O bearing phase, it could have been introduced during terrestrial alteration. If sphalerite did form during the formation of the QR, this would rely on either the reaction concentrating the (very limited) Zn from altered djerfisherite into sphalerite, or the introduction of small quantities of Zn during the reaction. However, no other elements appear to have been added during the QR reaction. On Earth, even in samples with very little overall weathering (i.e., the W0 NWA 13299 and SAH 97072), the QR was particularly susceptible to terrestrial alteration due to its porous microstructure. This led to the localized formation of the fibrous Fe-O bearing phase, along with Cu-sulfides in some weathered EH3-QRB (not observed in this study).

The transformation of djerfisherite to troilite resulted in a decrease in volume of the solid, leading to the development of pore space. We observed that remnant djerfisherite grains have different crystallographic orientations, compared to the primary, unaltered djerfisherite grain. This requires either the presence of polycrystalline djerfisherite as seen in FIB1 (Figure 7c,d) or a reorientation of the remnant djerfisherite during the formation of the QR.

The Environment in Which the QR Formed

In order to understand the QR further, we now attempt to understand the drivers for the QR reaction and implications for the environment of formation. Broadly speaking, there are three environments in which the QR could have formed: in the nebula (pre-accretion), on the EH parent body (post-accretion), or on Earth (relatively recent terrestrial weathering).

Pre-Accretion/Nebular Alteration

Although the exact formation mechanism is debated, chondritic djerfisherite is understood to have formed in the solar nebula (Ebel & Sack, 2013; El Goresy et al., 1988; Lin & El Goresy, 2002); therefore, it is worth considering the possibility that the QR also formed pre-accretion. We concluded earlier that djerfisherite-bearing opaque veins in the EH3 formed through shock processes, that is, post-accretion. In the EH3-QRB, the djerfisherite in any shock veins present also exhibits the QR. Additionally, we note that the QR is restricted only to EH meteorites and even then, only some EH3. This is despite djerfisherite being present, although more rarely, in some EL3. If the QR formed pre-accretion, we would expect it to be present in both EH3 and EL3; however, it is absent in the EL3. Therefore, it seems clear that the QR did not form prior to the accretion of the EH parent body, that is, in the nebula.

Terrestrial Weathering

Due to their reduced nature, ECs are particularly susceptible to terrestrial alteration. This raises the question as to whether terrestrial weathering caused the QR. As discussed earlier, we have already ruled out terrestrial weathering as a causal factor for the QR as there is no relationship between the degree of weathering or fall/find location and the presence/absence of the QR. Furthermore, an important argument against weathering causing the formation of the QR is the presence of pristine oldhamite which is sometimes found directly juxtaposed against the QR. Specifically, we observed this occurrence in both SAH 97072 and NWA 13299 (e.g., Figures 2b and 5d). Since oldhamite is extremely susceptible to terrestrial weathering (Piani et al., 2020; Weisberg & Prinz, 1998), the co-occurrence of oldhamite and the QR breakdown of djerfisherite indicates that very little terrestrial weathering has taken place. For all these reasons, we argue that the QR did not form as a result of terrestrial weathering.

EH Parent Body

The strongest evidence that the QR formed on the EH parent body is that it only occurs in EH meteorites, despite djerfisherite being found in other meteorite types (e.g., EL3, aubrites). Furthermore, by a process of elimination, the above arguments against nebular and weathering processes mean that the QR most likely formed post-accretion on the EH parent body. This environment potentially represents an approximately 4.5 Gyr period between the accretion of the parent body and the EH3-QRB meteorite falling to Earth. After accretion, the EH parent body went through significant changes, specifically thermal metamorphism, repeated impact processing, and disruption (sufficient to allow us to receive EH samples of all petrologic types on Earth). We now try to narrow the timing and environment of formation further.

In a related study, we developed a method to determine high and low petrologic subtypes for a range of EH3 chondrites, based primarily on the average Cr_2O_3 content of olivine, that is, high Cr_2O_3 content (>0.25 wt %) is observed in more primitive EH3 chondrites, and low Cr_2O_3 content (<0.25 wt%) in less primitive chondrites (Mc Ardle et al., 2025): see also Bendersky et al. (2007), Grossman and Brearley (2005), and Kimura et al. (2005). Mc Ardle et al. (2025) concluded that the EH3-QRB chondrites SAH 97072, NWA 13299, and Y-691 belong to the most primitive EH3 chondrites (what they called the $EH3_{Low}$ group). This is consistent with the conclusions of previous studies (Bendersky et al., 2007; Grossman & Brearley, 2005; Kimura et al., 2005). They also concluded that six other EH3 chondrites studied, mostly EH3-nonQRB but importantly including the EH3-QRB Qingzhen, fall into the more equilibrated group (which they called the $EH3_{High}$-EH4 group). This is also consistent with other studies that suggested that Qingzhen was more thermally metamorphosed than SAH 97072 (or its various pairings) (Hicks et al., 2000; Quirico et al., 2011), or that Qingzhen was more thermally metamorphosed than both SAH 97072 and Y-691 (Bendersky et al., 2007). If the formation of the QR was related to progressive thermal metamorphism, we might expect more metamorphosed samples to preferentially exhibit the QR, but this is not the case. Conversely, one might argue that the QR was somehow overprinted by thermal metamorphism, that is, all EH3 exhibited the QR at some point and metamorphism erases the evidence for this in the more highly metamorphosed samples. However, in this case, we would expect there to be no EH3-QRB in the more metamorphosed group (the $EH3_{High}$-EH4 group), and again this is not what is observed since QR is observed in Qingzhen. Therefore, we conclude that there is no direct relationship between the presence or absence of the QR in an EH3 and the degree of thermal metamorphism. As outlined earlier, we also rule out shock as a direct causal factor for the QR as there is no correlation between the degree of shock and the presence or absence of the QR.

This means there is still an approximately 4.5 Gyr window in which the QR could have formed. Although dates from both absolute (Ar-Ar, Rb-Sr) and relative (I-Xe, Mn-Cr) chronometers are available for the ECs, relatively little is known about the timing of the post-accretion history of the EC parent bodies (e.g., parent body disruption, the fate of EC material post disruption). Detailed chronology could be useful in determining the timing of the QR formation. Unfortunately, the chronology of the EH chondrites, particularly the EH3, is lacking data, and what data are available complicate the picture. The oldest dates obtained from EH3 are a Mn-Cr date of 4.565 Ga for the EH3-QRB SAH 97096 (Zhu et al., 2020), which Zhu et al. (2020) suggested was a chondrule formation age. Regarding I-Xe dates, Hopp et al. (2016) obtained whole rock dates of 4.555 Ga for the EH3-QRB SAH 97096, King et al. (2013) obtained dates of 4.565 Ga for djerfisherite from EH3-nonQRB ALHA77295, and Whitby et al. (2002) obtained dates of 4.563 Ga for chondrules in the EH3-QRB Qingzhen. Dates from absolute chronometers are sparser. In terms of Ar-Ar dating, attempts to date the EH3-QRB Y-691 did not produce meaningful dates (Honda et al., 1983). Hopp et al. (2014) obtained an apparent Ar-Ar date of 2.29 ± 0.07 Ga (based on a three point isochron) for the EH3-QRB SAH 97076. Rb-Sr dates of 2.12 ± 0.23 Ga and 2.05 ± 0.33 Ga were obtained for silicate fractions of the EH3-QRB Qingzhen and Y-691, respectively (Torigoye & Shima, 1993). We note that both these Ar-

Ar and Rb-Sr dates have considerable uncertainty and should be viewed as apparent dates. Note that only a single date for an EH3-nonQRB (ALHA77295) appears in the above chronology summary; the rest are from EH3-QRB. This is driven by the fact that the three most famous EH3 chondrites (Qingzhen, Y-691, and SAH 97072 [and pairings]) are all EH3-QRB. Both the Ar-Ar and Rb-Sr chronometers are largely controlled by djerfisherite, as it is the major K- and Rb-bearing phase in the EH3. It is, therefore, somewhat understandable that the Ar-Ar and Rb-Sr chronometers have been disturbed in the EH3-QRB, that is, a major K-carrier has broken down to produce the QR. Several authors have claimed that the younger apparent dates, c. 2 Ga, are linked to the formation of the QR (El Goresy et al., 1988; Hopp et al., 2014; King et al., 2013; Lin & El Goresy, 2002; Torigoye & Shima, 1993). Specifically, El Goresy et al. (1988) linked the QR and the young dates of the EH3-QRB to parent body thermal metamorphism, but stated this was problematic due to the young apparent dates. Hopp et al. (2014), King et al. (2013), Lin and El Goresy (2002), and Torigoye and Shima (1993), all linked the young apparent dates of the EH3-QRB, and the QR by association, to "late metamorphic events," with some suggesting heating from shock processes. In summary, the literature date converges on a c. 2 Ga date for the QR. However, given the uncertainties in the dating results and also the limited set of EH3 dated, particularly a lack of EH3-nonQRB, we suggest that it is not possible to confidently conclude that the QR formed at 2 Ga.

As noted earlier, little is known about the post-accretion history of the EH parent body. However, observations from polymict ureilites can assist. The ureilite parent body was catastrophically disrupted at ~5 Ma after CAI and the leftover material was then reassembled into secondary daughter bodies (Goodrich et al., 2024). Polymict ureilites, in particular Almahata Sitta, contain a range of clasts of non-ureilitic material, including EC material (Goodrich et al., 2024). Both EH- and EL-like samples are found in polymict ureilites (Goodrich et al., 2024; Weyrauch et al., 2018). Goodrich et al. (2024) suggested that this non-ureilitic material was implanted into ureilitic daughter bodies at ~50–60 Ma after CAI. According to this interpretation, by ~50–60 Ma after CAI, the EH (and also EL) parent body had been disrupted sufficiently to make EH material available to be incorporated into polymict ureilites. Perhaps at this time, two (or more) EH3 populations were isolated from each other in, for example, various EH rubble pile daughter bodies. In this scenario, two different, isolated, daughter bodies would evolve to become those with and without the QR. Sometime later (e.g., at 2 Ga), this may have allowed the QR to form in djerfisherite of the EH3-QRB daughter body but, for whatever reason, not on the EH3-nonQRB bearing daughter body/bodies.

This separate daughter body interpretation is appealing in that it provides a mechanism to separate the two populations of EH3, based on QR presence/absence. If this was not the case, it may be that the QR only formed on a portion of the EH parent body, as discussed below.

Proposed Formation Mechanism

We have discounted both thermal metamorphism and shock from impact processes as causal mechanisms for the formation of the QR. As observed by Lin and El Goresy (2002), kamacite-hosted djerfisherite does not show QR, which rather occurs along cracks and grain boundaries, suggesting that the mechanism that triggered the formation of the QR could only interact with djerfisherite outside of metal. These observations are consistent with an external fluid (liquid or gas), which infiltrated the rock and caused the formation of the QR. Notably it is always the edges of djerfisherite grains that exhibit the QR, with unaltered djerfisherite often found at the cores (e.g., Figure 5). This is also consistent with a fluid causing the QR, and indeed that the reaction was fluid limited, because the QR did not completely alter all djerfisherite in all cases. The open system nature of the reaction also supports the involvement of a fluid, with K, Cu, Ni, and Cl having been transported away from the site of the QR.

Hydrous fluids were abundant in the early solar system, particularly in the CM and CI carbonaceous chondrite groups as well as in ordinary chondrites (Grant et al., 2023; Marrocchi et al., 2018). For ECs, Piani et al. (2020) quantified the indigenous H content, while Barrett et al. (2025) suggested that H bonded to S was the dominant speciation. Evidence for aqueous alteration of the EC parent bodies is very rare, although some possible hydrothermal alteration products have been described in two anomalous EL3 (or EL3-related) chondrites. The EL3 NWA 8785 contains a magnetite-rich matrix and sodalite (Rindlisbacher et al., 2021; Weisberg et al., 2023). Additionally, in the anomalous EL3-related EC LEW 87223, Goss et al. (2023) found evidence of Na metasomatism in the form of abundant aluminum-rich chondrules with both Ca and Na-plagioclase. However, the alteration products in those anomalous EL3 are very different from what we observe in the EH3-QRB. In the case of the QR, we can rule out a meteoritical hydrous fluid due to the presence of pristine oldhamite juxtaposed directly against the QR in both SAH 97072 and NWA 13299. Therefore, we conclude that the fluid in question was an anhydrous fluid. Possible fluids include carbon

monoxide, methane, hydrogen, and hydrogen sulfide. The presence of reducing, anhydrous fluids has also been suggested based on studies of CAIs in the EH3 chondrite, Sahara 97,159 (paired with SAH 97072) (Lin et al., 2003).

We consider two possible sources for the anhydrous fluid involved in the QR: degassing from the interior of the EH parent body or development/introduction via an impact event. In the first scenario, the QR formed contemporaneously with or just after EH parent body metamorphism. In this scenario, thermal metamorphism could have driven degassing from the interior (e.g., depths at which the EH6 formed) and provided the anhydrous fluid, which preferentially rose to the EH parent body surface (i.e., site for the EH3) in only one region, that is, where the EH3-QRB formed. The remainder of the EH parent body surface would be the source of the EH3-nonQRB. It is well-known that thermal metamorphism results in volatile loss in the ECs: Clay et al. (2017) showed halogen loss with progressive metamorphism, while Piani et al. (2020) showed H loss with progressive metamorphism. The degassing model which we propose would seem to require the formation of the QR relatively early (e.g., 4.4–4.5 Ga), which would not be consistent with the 2 Ga apparent dates of the EH3-QRB (Hopp et al., 2014; Torigoye & Shima, 1993), although these c. 2 Ga dates are poorly constrained. In the second scenario we consider, the anhydrous fluid was generated on the EH parent body (or post break up daughter body) surface as a result of impacts, for example, fluid produced through degassing of an impact melt sheet. Gray et al. (2025) suggested that metamorphism on the EH parent body was driven by impact melt sheets. However, it is important to consider that the EH3-QRB studied here and elsewhere (El Goresy et al., 1988; Lin & El Goresy, 2002) are only weakly to moderately shocked, constraining the extent of the shock processes to which these meteorites were exposed.

Both the scenarios above are speculative, although they are conceptually feasible. However, we are not currently able to determine which is preferred, as we cannot narrow down the details of the fluid further based on the data available.

We note that whichever of these QR-generating scenarios occurred on the EH parent body, the same situation did not apparently occur on the EL or aubrite parent bodies. Even though djerfisherite is rarer in EL chondrites and aubrites it does still occur, and none of that djerfisherite exhibits the QR.

CONCLUSIONS

The Qingzhen Reaction is a fine-grained mineral assemblage associated with the K- and Cl-bearing sulfide mineral, djerfisherite, in some EH3 chondrites. We examined the chemistry and fine-grained mineralogy of the Qingzhen reaction (QR) and associated djerfisherite using SEM-EDS, TEM, TKD, and LA-ICPMS. Our study focused on two EH3-QRB: SAH 97072 and NWA 13299. When present in a given EH3 chondrite, the QR is present in all mineralogical associations of djerfisherite in that meteorite, including shock veins, with the exception of djerfisherite inclusions in metal grains. Our analysis shows that troilite formed as the main in situ product of the QR, at the expense of djerfisherite. Rare halite grains formed contemporaneously. Extremely rare and small sphalerite grains may also have formed in the QR; alternatively, they may also have been inclusions within the precursor djerfisherite. Remnant djerfisherite, not broken down during the QR reaction, remained as islands in the newly formed QR. The elements K, Cu, Ni, and Cl were largely lost from the djerfisherite during the formation of the QR and transported away from the reaction site, likely into the surrounding matrix/chondrules. There is no relationship between the shock stage or weathering grade of an EH3 and the presence or absence of the QR. On Earth, even in samples with very little overall weathering, (i.e., the W0 NWA 13299 and SAH 97072), the QR was particularly susceptible to terrestrial alteration due to its porous microstructure. This led to the localized formation of the fibrous Fe-O bearing phase, along with Cu-sulfides (covellite, bornite, and idaite) in some weathered EH3-QRB. We conclude that the QR formed on the EH parent body, or on a daughter body following the breakup of the original EH body. The QR was likely formed in response to the alteration of djerfisherite by a fluid phase that was anhydrous, based on the presence of adjacent oldhamite which is highly susceptible to aqueous alteration. The reaction was fluid-limited, as it did not go to completion in most cases. Possible sources of such a fluid include degassing from the interior of the EH parent body during thermal metamorphism, or generation of a fluid as a result of impacts closer to the parent body surface. Formation of the QR may be related to young dates c. 2 Ga for EH3-QRB chondrites. This would argue for an origin related to impacts rather than thermal metamorphism, although the age of formation of the QR itself is currently poorly constrained.

Acknowledgments—We thank the various meteorite hunters/dealers/collectors for sourcing the samples included in this study. We thank the classifiers for working on these samples. We thank the following individuals and institutions for providing samples; The Antarctic Search for Meteorites/NASA/JSC, National Institute for Polar Research, University of California Los Angeles Meteorite Collection, F. Kuntz (WW Meteorites), and E. Twelker (The Meteorite Market).

RHJ acknowledges funding through UK Science and Technology Facilities Council (STFC) grant ST/V000675/1. LD acknowledges funding through UK STFC grant ST/W001128/1. RT acknowledges STFC (grant #ST/S002170/1) and the University of Manchester for funding the LA-ICPMS facility in Manchester. PLC thanks Henner Busemann for discussions on the formation of djerfisherite in enstatite chondrites. BO'D acknowledges current research support from the Natural Sciences and Engineering Research Council of Canada (NSERC Discovery Grant) and from the Newmont Chair in Economic Geology (University of Ottawa).

Data Availability Statement—The data that support the findings of this study are openly available in FigShare at http://doi.org/10.48420/29314406.

Editorial Handling—Dr. Michael Zolensky

REFERENCES

Barrett, T. J., Bryson, J. F., and Geraki, K. 2025. The Source of Hydrogen in Earth's Building Blocks. *Icarus* 436: 116588.

Bendersky, C., Weisberg, M. K., Jr., Connolly, H. C., and Ebel, D. S. 2007. Olivine and the Onset of Thermal Metamorphism in EH3 Chondrites. *38th Lunar and Planetary Science* Conference, p. 2077.

Bestmann, M., and Prior, D. J. 2003. Intragranular Dynamic Recrystallization in Naturally Deformed Calcite Marble: Diffusion Accommodated Grain Boundary Sliding as a Result of Subgrain Rotation Recrystallization. *Journal of Structural Geology* 25: 1597–1613.

Brearley, A., and Jones, R. H. 2018. Halogens in Chondritic Meteorites. In *The Role of Halogens in Terrestrial and Extraterrestrial Geochemical Processes Surface, Crust, and Mantle*, edited by D. E. Harlov, and L. Aranovich, 871–958. Switzerland: Springer Geochemistry.

Clay, P. L., Burgess, R., Busemann, H., Ruzie-Hamilton, L., Joachim, B., Day, J. M. D., and Ballentine, C. J. 2017. Halogens in Chondritic Meteorites and Terrestrial Accretion. *Nature* 551: 614–18.

Clay, P. L., O'Driscoll, B., Upton, B. G. J., and Busemann, H. 2014. Characteristics of Djerfisherite from Fluid-Rich, Metasomatized Alkaline Intrusive Environments and Anhydrous Enstatite Chondrites and Achondrites. *American Mineralogist* 99: 1683–93.

Ebel, D. S., and Sack, R. O. 2013. Djerfisherite: Nebular Source of Refractory Potassium. *Contributions to Mineralogy and Petrology* 166: 923–934.

El Goresy, A. 1971. Djerfisherite Composition in Bishopsville, Pena Blanca Springs, St. Marks and Toluca Meteorites. *Chemie der Erde* 30: 77–82.

El Goresy, A. 1985. The Qinzhen Reaction: Fingerprints of the EH Planet? *Meteoritics* 20: 639.

El Goresy, A., and Ehlers, K. 1989. Sphalerites in EH Chondrites: I. Textural Relations, Compositions, Diffusion Profiles, and Pressure-Temperature Histories. *Geochimica et Cosmochimica Acta* 53: 1657–68.

El Goresy, A., Yabuki, H., Ehlers, K., Woolum, D., and Pernicka, E. 1988. Qingzhen and Yamato-691: A Tentative Alphabet for the EH Chondrites Proceedings of the NIPR Symposium. Antarctic Meteorites, 1, 65–101.

El Goresy, A., Yabuki, H., and Pernicka, E. 1983. Qinzhen: A Tentative Alphabet for the Enstatite Chondrite Clan. *Meteoritics* 18: 293.

Elburg, M., Vroon, P., van der Wagt, B., and Tchalikian, A. 2005. Sr and Pb Isotopic Composition of Five USGS Glasses (BHVO-2G, BIR-1G, BCR-2G, TB-1G, NKT-1G). *Chemical Geology* 223: 196–207.

Erokhin, Y. V., Koroteev, V. A., Khiller, V. V., Ivanov, K. S., and Kleimenov, D. A. 2018. The Severny Kolchim Meteorite: New Data on Mineralogy. *Doklady Earth Sciences* 482: 1189–92.

Forman, L., Bland, P., Timms, N., Collins, G., Davison, T., Ciesla, F., Benedix, G., Daly, L., Trimby, P., and Yang, L. 2016. Hidden Secrets of Deformation: Impact-Induced Compaction within a CV Chondrite. *Earth and Planetary Science Letters* 452: 133–145.

Fuchs, L. H. 1966. Djerfisherite, Alkali Copper-Iron Sulfide: A New Mineral from Enstatite Chondrites. *Science* 153: 166–67.

Goodrich, C. A., Downes, H., Greenwood, R., Ross, A. J., Fioretti, A. M., Alexander, L., Kita, N. T., Butler, J., Jercinovic, M. J., and Jenniskens, P. 2024. Enstatite Meteorite Clasts in Almahata Sitta and Other Polymict Ureilites: Implications for the Formation of Asteroid 2008 TC3 and the History of Enstatite Meteorite Parent Asteroids. *Meteoritics & Planetary Science* 59: 719–753.

Goss, K. R., Gray, M. L., Weisberg, M. K., and Ebel, D. S. 2023. Lewis Cliff 87223, an Anomalous Enstatite Chondrite and the Diversity of Enstatite Chondrites. *Meteoritics & Planetary Science* 58: 433–443.

Grant, H., Tartèse, R., Jones, R., Piani, L., Marrocchi, Y., King, A., and Rigaudier, T. 2023. Bulk Mineralogy, Water Abundance, and Hydrogen Isotope Composition of Unequilibrated Ordinary Chondrites. *Meteoritics & Planetary Science* 58: 1365–81.

Gray, M. L., Weisberg, M. K., Jaret, S. J., and Ebel, D. S. 2025. EH6 enstatite Chondrites Northwest Africa 7976 and Northwest Africa 12945: Implications for EH Chondrite Metamorphism. *Meteoritics & Planetary Science* 60: 51–63.

Grossman, J. N., and Brearley, A. J. 2005. The Onset of Metamorphism in Ordinary and Carbonaceous Chondrites. *Meteoritics & Planetary Science* 40: 87–122.

Hicks, T. L., Fagan, T. J., and Keil, K. 2000. Metamorphic Sequence of Unequilibrated EH Chondrites Using Modal Olivine and Silica Abundance. *31st Lunar and Planetary Science*, p. 1491.

Honda, M., Bernatowicz, T. J., and Podoesk, F. A. 1983. Xe-129 - Xe-128 and Ar-40 - Ar-39 Chronology of Two Antarctic Enstatite Meteorites. *Memiors of National Institute of Polar Research* 30: 113–121.

Hopp, J., Trieloff, M., and Ott, U. 2016. I–Xe Ages of Enstatite Chondrites. *Geochimica et Cosmochimica Acta* 174: 196–210.

Hopp, J., Trieloff, M., Ott, U., Korochantseva, E. V., and Buykin, A. I. 2014. ^{39}Ar-^{40}Ar Chronology of the Enstatite Chondrite Parent Bodies. *Meteoritics & Planetary Science* 49: 358–372.

Huss, G. R., Rubin, A. E., and Grossman, J. N. 2006. Thermal Metamorphism in Chondrites. In *Meteorites and*

the Early Solar System II, vol. 943, 567–586. Tuscon: The University of Arizona Press.

Jacquet, E., Piani, L., and Weisberg, M. 2018. Chondrules in Enstatite Chondrites. In *Chondrules: Records of Protoplanetary Disk Processes*, 175–195. Cambridge: Cambridge University Press.

Jochum, K. P., Nohl, U., Herwig, K., Lammel, E., Stoll, B., and Hofmann, A. W. 2005. GeoReM: A New Geochemical Database for Reference Materials and Isotopic Standards. *Geostandards and Geoanalytical Research* 29: 333–38.

Jochum, K. P., Willbold, M., Raczek, I., Stoll, B., and Herwig, K. 2005. Chemical Characterisation of the USGS Reference Glasses GSA-1G, GSC-1G, GSD-1G, GSE-1G, BCR-2G, BHVO-2G and BIR-1G Using EPMA, ID-TIMS, ID-ICP-MS and LA-ICP-MS. *Geostandards and Geoanalytical Research* 29: 285–302.

Kimura, M., Lin, Y.-T., Ikeda, Y., Goresy, A. E., Yanai, K., and Kojima, H. 1993. Mineralogy of Antarctic Aubrites, Yamato-793592 and Allan Hills-78113: Comparison with Non-Antarctic Aubrites and E-Chondrites. In *Proceedings of the NIPR Symposium on Antarctic Meteorites*, 186–203. Toyko: National Institute of Polar Research.

Kimura, M., Weisberg, M. K., Lin, Y., Suzuki, A., Ohtani, E., and Okazaki, R. 2005. Thermal History of the Enstatite Chondrites from Silica Polymorphs. *Meteoritics & Planetary Science* 40: 855–868.

King, A. J., Clay, P. L., Crowther, S. A., Nottingham, M., Gilmour, J. D., Wieler, R., and Busemann, H. 2013. Noble Gas Chronology of EH3 Chondrite ALHA77295 by Closed System Stepped Etching. 44th Lunar and Planetary Science Conference, p. 2217.

Kleine, T., Budde, G., Burkhardt, C., Kruijer, T., Worsham, E., Morbidelli, A., and Nimmo, F. 2020. The Non-Carbonaceous–Carbonaceous Meteorite Dichotomy. *Space Science Reviews* 216: 1–27.

Kracher, A., Kurat, G., and Vf, B. 1977. Cape York: The Extraordinary Mineralogy of an Ordinary Iron Meteorite and its Implication for the Genesis of III AB Irons. *Geochemical Journal* 11: 207–217.

Lee, M., Bland, P., and Graham, G. 2003. Preparation of TEM Samples by Focused Ion Beam (FIB) Techniques: Applications to the Study of Clays and Phyllosilicates in Meteorites. *Mineralogical Magazine* 67: 581–592.

Lehner, S. W., Petaev, M. I., Zolotov, M. Y., and Buseck, P. R. 2013. Formation of Niningerite by Silicate Sulfidation in EH3 Enstatite Chondrites. *Geochimica et Cosmochimica Acta* 101: 34–56.

Lin, Y. 2022. Enstatite Chondrites: Condensation and Metamorphism under Extremely Reducing Conditions and Contributions to the Earth. *Progress in Earth and Planetary Science* 9: 16.

Lin, Y., and El Goresy, A. 2002. A Comparative Study of Opaque Phases in Qingzhen (EH3) and MacAlpine Hills 88136 (EL3): Representatives of EH and EL Parent Bodies. *Meteoritics & Planetary Science* 37: 577–599.

Lin, Y., Kimura, M., Hiyagon, H., and Monoi, A. 2003. Unusually Abundant Refractory Inclusions from Sahara 97159 (EH3): A Comparative Study with Other Groups of Chondrites. *Geochimica et Cosmochimica Acta* 67: 4935–48.

Macke, R. J., Consolmagno, G. J., Britt, D. T., and Hutson, M. L. 2010. Enstatite Chondrite Density, Magnetic Susceptibility, and Porosity. *Meteoritics & Planetary Science* 45: 1513–26.

Marrocchi, Y., Bekaert, D. V., and Piani, L. 2018. Origin and Abundance of Water in Carbonaceous Asteroids. *Earth and Planetary Science Letters* 482: 23–32.

Mc Ardle, P., Jones, R. H., Clay, P., Tartèse, R., Burgess, R., O'Driscoll, B., Hellebrand, E. W. G., Fellowes, J., Goodwin, A., and Hughes, L. 2025. Parent Body Thermal Metamorphism of Enstatite Chondrites: Disentangling the Effects of Shock Melting. *Meteoritics & Planetary Science* https://doi.org/10.1111/maps.70065

Minster, J. F., Ricard, L. P., and Alliegre, C. J. 1979. $^{87}Rb/^{87}Sr$ Chronology of Enstatite Meteorites. *Earth and Planetary Science Letters* 44: 420–440.

Miyahara, M., Noguchi, T., Yamaguchi, A., Nakahashi, T., Takaki, Y., Matsumoto, T., Tomioka, N., Miyake, A., Igami, Y., and Seto, Y. 2025. Djerfisherite in a Ryugu Grain: A Clue to Localized Heterogeneous Conditions or Material Mixing in the Early Solar System. *Meteoritics & Planetary Science* 60: 1666–73.

Palme, H., Lodders, K., and Jones, A. 2014. Solar System Abundances of the Elements. In *Planets, Asteriods, Comets and the Solar System, Volume 2 of Treatise on Geochemistry*, edited by A. M. Davis, 2nd ed., 15–36. Amsterdam: Elsevier.

Paton, C., Hellstrom, J., Paul, B., Woodhead, J., and Hergt, J. 2011. Iolite: Freeware for the Visualisation and Processing of Mass Spectrometric Data. *Journal of Analytical Atomic Spectrometry* 26: 2508–18.

Piani, L., Marrocchi, Y., Rigaudier, T., Vacher, L. G., Thomassin, D., and Marty, B. 2020. Earth's Water May Have Been Inherited from Material Similar to Enstatite Chondrite Meteorites. *Science* 369: 1110–13.

Quirico, E., Bourot-denise, M., Robin, C., Montagnac, G., and Beck, P. 2011. A Reappraisal of the Metamorphic History of EH3 and EL3 Enstatite Chondrites. *Geochimica et Cosmochimica Acta* 75: 3088–3102.

Ramdohr, P. 1963. The Opaque Minerals in Stony Meteorites. *Journal of Geophysical Research* 68: 2011–36.

Rindlisbacher, M. A., Weisberg, M. K., Ebel, D. S., Alpert, S. P., and Brearley, A. 2021. Metal-Rich Nodules in Anomalous EL3 Chondrite Northwest Africa (NWA) 8785. *Meteoritics & Planetary Science* 56: 960–970.

Rubin, A. E. 1997. Mineralogy of Meteorite Groups. *Meteoritics & Planetary Science* 32: 231–247.

Rubin, A. E. 2015. Impact Features of Enstatite Rich Meteorites. *Chemie der Erde* 75: 1–28.

Rubin, A. E., and Choi, B.-G. 2009. Origin of Halogens and Nitrogen in Enstatite Chondrites. *Earth, Moon, and Planets* 105: 41–53.

Rubin, A. E., and Wasson, J. T. 2011. Shock Effects in "EH6" enstatite Chondrites and Implications for Collisional Heating of the EH and EL Parent Asteroids. *Geochimica et Cosmochimica Acta* 75: 3757–80.

Sugiura, N., and Fujiya, W. 2014. Correlated Accretion Ages and 54Cr of Meteorite Parent Bodies and the Evolution of the Solar Nebula. *Meteoritics & Planetary Science* 49: 772–787.

Torigoye, N., and Shima, M. 1993. Evidence for a Late Thermal Event of Unequilibrated Enstatite Chondrites: A Rb-Sr Study of Qingzhen and Yamato 6901 (EH3) and Khairpur (EL6). *Meteoritics* 28: 515–527.

Trimby, P. W. 2012. Orientation Mapping of Nanostructured Materials Using Transmission Kikuchi Diffraction in the

Scanning Electron Microscope. *Ultramicroscopy* 120: 16–24.

Wang, Y., Han, X., Petersen, S., Jin, X., Qiu, Z., and Zhu, J. 2014. Mineralogy and Geochemistry of Hydrothermal Precipitates from Kairei Hydrothermal Field, Central Indian Ridge. *Marine Geology* 354: 69–80.

Weisberg, M. K., and Kimura, M. 2012. The Unequilibrated Enstatite Chondrites. *Chemie der Erde* 72: 101–115.

Weisberg, M. K., and Prinz, M. 1998. Sahara 97096: A Highly Primitive EH3 Chondrite with Layered Sulfide-Metal-Rich Chondrules. *29th Lunar and Planetary Science Conference*, p. 1741.

Weisberg, M. K., Zolensky, M. E., Kimura, M., Howard, K. T., Ebel, D. S., Gray, M. L., and Alexander, C. M. O.'D. 2023. Nanophase Magnetite in Matrix of Anomalous EL3 Chondrite Northwest Africa (NWA) 8785. *Meteoritics & Planetary Science* 58: 1693–1706.

Weyrauch, M., Horstmann, M., and Bischoff, A. 2018. Chemical Variations of Sulfides and Metal in Enstatite Chondrites-Introduction of a New Classification Scheme. *Meteoritics & Planetary Science* 53: 394–415.

SUPPORTING INFORMATION

Additional supporting information may be found in the online version of this article.

Whitby, J. A., Gilmour, J. D., Turner, G., Prinz, M., and Ash, R. D. 2002. Iodine-Xenon Dating of Chondrules from the Qingzhen and Kota Kota Enstatite Chondrites. *Geochimica et Cosmochimica Acta* 66: 347–359.

Wilbur, Z. E., McCoy, T. J., Corrigan, C. M., Barnes, J. J., Brown, S. V., and Udry, A. 2024. The Formation of Volatile-Bearing Djerfisherite in Reduced Meteorites. *Meteoritics & Planetary Science* 59: 2373–87.

Woodhead, J. D., and Hergt, J. M. 2001. Strontium, Neodymium and Lead Isotope Analyses of NIST Glass Certified Reference Materials: SRM 610, 612, 614. *Geostandards Newsletter* 25: 261–66.

Zhu, K., Moynier, F., Schiller, M., and Bizzarro, M. 2020. Dating and Tracing the Origin of Enstatite Chondrite Chondrules with Cr Isotopes. *The Astrophysical Journal Letters* 894(L26): 1–9.

Zurfluh, F. J., Hofmann, B. A., Gnos, E., Eggenberger, U., and Jull, A. J. T. 2016. Weathering of Ordinary Chondrites from Oman: Correlation of Weathering Parameters with 14C Terrestrial Ages and a Refined Weathering Scale. *Meteoritics & Planetary Science* 51: 1685–1700.

Data S1. LA-ICP-MS Data for EH3 Enstatite Chondrites.